ANALYTIC AND NUMERICAL MODELING OF HEAT AND MATERIAL
TRANSPORT IN ELECTRI. .(U) GT-DEVICES INC ALEXANDRIA VA
N K WINSOR 04 DEC 87 AFOSR-TR-88-0257 F49620-85-C-0134

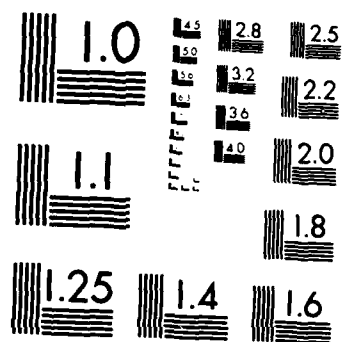F/G 20/3   NL

END
FILMED

DTIC

MICROCOPY RESOLUTION TEST CHART
NATIONAL BUREAU OF STANDARDS-1963-A
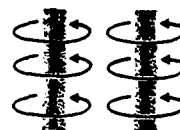
AFOSR-TR- 88-0257

ANALYTIC AND NUMERICAL MODELING

OF HEAT AND MATERIAL TRANSPORT

IN ELECTRIC HYPERVELOCITY GUNS

Contract F49620-85-C-0134

GT - Devices

DTIC
ELECTE
MAR 09 1988
S D
D.

5705A General Washington Drive   Alexandria, VA 22312   (703) 642-8150

88   3   7   127

ANALYTIC AND NUMERICAL MODELING

OF HEAT AND MATERIAL TRANSPORT

IN ELECTRIC HYPERVELOCITY GUNS

Contract F49620-85-C-0134

Final Report

For the Period 4 Sep 1986 - 5 Sep 1986

By

GT-Devices, Inc.
5705A General Washington Drive
Alexandria, VA   22312

To

United States Air Force
Office of Scientific Research
Building 410
Bolling AFB, DC 20332-6448

December 4, 1987

REPORT DOCUMENTATION PAGE

1a. REPORT SECURITY CLASSIFICATION	1b. RESTRICTIVE MARKINGS
2a. SECURITY CLASSIFICATION AUTHORITY	**3. DISTRIBUTION/AVAILABILITY OF REPORT**
2b. DECLASSIFICATION/DOWNGRADING SCHEDULE	Approved for public release, distribution unlimited

4. PERFORMING ORGANIZATION REPORT NUMBER(S)	5. MONITORING ORGANIZATION REPORT NUMBER(S) AFOSR·TR· 88-0257

6a. NAME OF PERFORMING ORGANIZATION GT-Devices, Inc.	6b. OFFICE SYMBOL (If applicable) 7T674	7a. NAME OF MONITORING ORGANIZATION AFOSR
6c. ADDRESS (City, State, and ZIP Code) 5705A General Washington Drive Alexandria, VA 22312-2408		7b. ADDRESS (City, State, and ZIP Code) same as 7c.

8a. NAME OF FUNDING/SPONSORING ORGANIZATION AFOSR	8b. OFFICE SYMBOL (If applicable) NP	9. PROCUREMENT INSTRUMENT IDENTIFICATION NUMBER F49620-85-C-0134

| 8c. ADDRESS (City, State, and ZIP Code) Air Force Office of Scientific Research Building 410, Bolling AFB, DC 20332-6448 | 10. SOURCE OF FUNDING NUMBERS |

PROGRAM ELEMENT NO.	PROJECT NO.	TASK NO.	WORK UNIT ACCESSION NO.
61102F	2301	A8	

11. TITLE (Include Security Classification)

Analytic and Numerical Modeling of Heat and Material Transport in Electric Hypervelocity Guns

12. PERSONAL AUTHOR(S)   Niels K. Winsor

13a. TYPE OF REPORT Final Annual Report	13b. TIME COVERED FROM 86/09/05 TO 87/09/06	14. DATE OF REPORT (Year, Month, Day) December 4, 1987	15. PAGE COUNT 40

16. SUPPLEMENTARY NOTATION

17. COSATI CODES			18. SUBJECT TERMS (Continue on reverse if necessary and identify by block number)
FIELD	GROUP	SUB-GROUP	hypervelocity, electrothermal, electromagnetic, rail, gun, erosion, ablation

19. ABSTRACT (Continue on reverse if necessary and identify by block number)

A computer simulation code has been developed. The physical transport processes of radiation transport, viscosity, electrical and thermal conductivity and turbulence were included in the study. The code benchmarked against material erosion experiments with metals and insulators. The processes occurring near the bore wall of an electro-thermal gun have been evaluated. The studies have demonstrated the utility of a gun system redesign which lowers the propelling gas temperature near the wall. This has resulted in the experimental reduction of gun bore erosion to levels at or below the erosion in conventional powder guns. The code results have also been interpreted for the electromagnetic (rail) gun case. Here the unavoidable high propelling gas temperatures cause a more severe erosion problem.

20. DISTRIBUTION/AVAILABILITY OF ABSTRACT ☐ UNCLASSIFIED/UNLIMITED ☒ SAME AS RPT. ☐ DTIC USERS	21. ABSTRACT SECURITY CLASSIFICATION Unclassified
22a. NAME OF RESPONSIBLE INDIVIDUAL Dr. Robert J. Barker	22b. TELEPHONE (Include Area Code) (202) 767-5011	22c. OFFICE SYMBOL NP

DD FORM 1473, 84 MAR   83 APR edition may be used until exhausted.   SECURITY CLASSIFICATION OF THIS PAGE

All other editions are obsolete.

Technical Summary

An experimentally benchmarked FORTRAN computer code has been developed for the VAX computer. This simulation code treats the dynamic processes occurring in the interior of electric gun systems. It pays special attention to the processes occurring in the boundary layer between the hot plasma flow and the solid "wall" of the gun barrel bore.

This code has been used to study the physical processes involved in the wall erosion problem in electric gun systems. This includes heat transport into and through the very thin boundary layer and the effect of this heat transmission on the wall material.

An analytical model of the flow and transport in an electrothermal gun has been developed. This model accurately predicts many of the features of the heat transport to the wall. This process is the primary cause of erosion in the gun bore. A report describing this model is presented as Appendix A.

The code has been benchmarked against laboratory experiments at GT-Devices. In these experiments, plasma flows were produced which approximated both the propellant in an electrothermal gun and the armature in a rail gun. These flows were directed past samples of gun bore material, and the ablation of the material was measured. Since the properties of the plasma flow were known, the heat transport through the skin layer to the sample could be calculated. The comparison benchmarks the calculations.

In the case of the Electrothermal gun, the study of these processes has led to a change in the design of the gun which has virtually eliminated the wall erosion problem for many projectile masses and velocities of military interest. The required change is the addition of a "mixing chamber" between the capillary which is the source of hot plasma and the barrel, which requires a cooler environment.

The understanding which has been developed for the wall erosion problem has been extended to the Electromagnetic (rail) gun geometry. The heat sources internal to a rail gun lead to higher heat loads on the rail gun wall for projectile parameters of military interest. This heat load is delivered both to the metal rails and to the insulators between them. The effect on these components is to cause ablation.

iii

Contract Summary

(a) The statement of work for this program is:

This principal desired outcome of this overall project is an experimentally benchmarked, VAX-compatible, FORTRAN (or PASCAL) computer simulation code which will treat in a physically validated fashion the dynamic processes occurring in the boundary layer between a dense, high temperature plasma and a solid "wall." The code will employ a number of asymptotically coupled, one-dimensional algorithms to treat both the fast timescale processes perpendicular to the wall as well as the much slower timescale plasma flow along the wall. This code will be used to enhance the physical understanding of the wall erosion problem in electrothermal guns and will be available for possible application to the rail erosion problem in electromagnetic launchers by other research efforts. The desired research milestones for each of the three years include the following:

Determine the appropriate transport coefficients to be used in the electrothermal jet and in the wall boundary layer including the Rosseland opacity for radiation transport, the viscosity, and the electrical and thermal conductivities for the partially ionized plasma. Also, integrate these transport coefficients into a VAX-compatible, FORTRAN (or PASCAL) code which contains the flow algorithms for the boundary in the gun barrel. The resultant code will be used to simulate systems with experimentally relevant parameters and the results will be compared to empirical data available from electrothermal guns presently in operation. An annual report will be delivered to AFOSR which will discuss the algorithms contained in the code, will summarize the findings of the comparison with experimental data and will include a complete copy of the FORTRAN (or PASCAL) source file of the code(s) on an IBM-PC compatible diskette.

Option 1:

Based on the experimental comparisons, evaluate the importance of turbulence in the erosion process. If necessary, incorporate a turbulent boundary layer algorithm in the code. Conduct a series of simulations for a range of electrothermal gun parameters, electrical power levels, and materials. Determine the dependencies of the gun performance parameters to these changes. Submit an annual report to AFOSR to present the major results of the above work. The report should include an IBM-PC compatible diskette(s) containing a complete copy of the FORTRAN (or PASCAL) source file of the latest, updated version of the simulation code(s).

Option 2:
Incorporate into the code(s) output routines which will generate graphical displays of the solutions so that the dynamics can be visualized. Use the computer simulation results to derive some general scaling relationships for the dynamic behavior of the plasma jets. Submit a final report for AFOSR which will include a compilation of simulation results and the derived scaling relationships that would be useful for applications of these electrothermal jets to hypervelocity launchers and to other applications. This final report will include a complete copy of the FORTRAN (or PASCAL) source file of the latest, updated version of the simulation code on an IBM-PC compatible diskette as well as complete documentation for the code's algorithms and instructions for its use.

(b) Status of the research effort:
All the milestones of the initial task and option 1 have been met. Option 2 has not been exercised. Activity under the contract has been completed. The experimentally benchmarked, VAX-compatible FORTRAN computer simulation code has been developed. This code was used to enhance the physical understanding of wall erosion. The transport coefficients for Rosseland opacity, viscosity, electrical and thermal conductivity and turbulence have been incorporated. Simulations have been performed which are relevant to both electrothermal guns and electromagnetic (rail) guns. This final report has been submitted. A complete copy of the FORTRAN source file is included with the copies of the report, on a DOS 3 formatted 5-1/4" 360k diskette.

(c) No journal articles have been prepared or published; however, a technical report,
"Gun Interior Ballistics Model for Constant Acceleration Launch of Projectiles," by D. A. Tidman, N. K. Winsor and S. A. Goldstein, GT-Devices Technical Note GTD 86-2, dated February 1986,
has been prepared and distributed. It is included here as Appendix A.

(d) The professional personnel associated with the program are:
Dr. Niels K. Winsor
Dr. Derek A. Tidman
Dr. Shyke A. Goldstein
Dr. Howard W. Bloomberg
No advanced degrees have been awarded.

(e) Interactions:
1. Paper presented by N. K. Winsor, titled "The Gun Bore Bearing in EM and ET Launchers," by N.K. Winsor, D.A. Tidman,S.A. Goldstein and H.W. Bloomberg, presented at <u>Innovative Science and Technology Electromagnetic Launch Science Interchange Workshop</u>, Eglin AFB, 23 June 1986.
2. Paper presented by D. A. Tidman, titled "A Rail Gun Plasma Armature Model," at the <u>Electromagnetic Gun Armature Workshop</u>, Eglin Air Force Base, 24-26 June 1986.
3. Half-day seminar-workshop presented by N. K. Winsor and Y. Chia Thio, to Eglin AFB and Auburn University personnel on "Electromagnetic and Electrothermal Research at GT-Devices," Eglin Air Force Base, 21-22 August 1986.

(f) New discoveries, inventions, or patent disclosures and specific applications stemming from the research effort:
In conjunction with experiments, these simulations aided in interpreting the erosion phenomena in the GT-Devices 20 mm Electrothermal gun. The synergism of these studies provided the insight necessary to redesign the breech chamber of the gun and substantially eliminate the erosion problem for most applications of military interest.

(g) Any other statements:
See balance of report!

Acknowledgements

Table of contents

List of figures

List of tables

x

Introduction

The performance of an airborne gun significantly affects the kind of mission the aircraft can accomplish. For example, the C-130 gunship is designed for use in an orbit around a selected target. A higher velocity gun can mean the difference between an orbit within range of ground fire and a position well outside the range of the ground defense. (See Figure 1.) The higher velocity can also simplify fire control when engaging a moving target.

For conventional powder guns, a practical velocity limit for long-life service is around 1 km/sec (3300 ft/sec). For example, this is close to the performance of the Phalanx close-in shipboard defense system, which has been designed for high velocity and rapid fire.

Chemical propellants are capable of higher velocities, but when such performance is achieved, it is at considerable cost, usually in a much larger chemical charge, greatly increased barrel wear and complex projectile designs, often including a discarding sabot.

The Strategic Defense Initiative has motivated the search for methods to achieve much higher velocity with gun systems. One result has been increased research on electric gun systems, principally the electromagnetic (rail) gun.

More recently, the electrothermal gun has been receiving attention as a gun with many of the advantages of the rail gun, while avoiding most of the disadvantages of other kinds of electric guns.
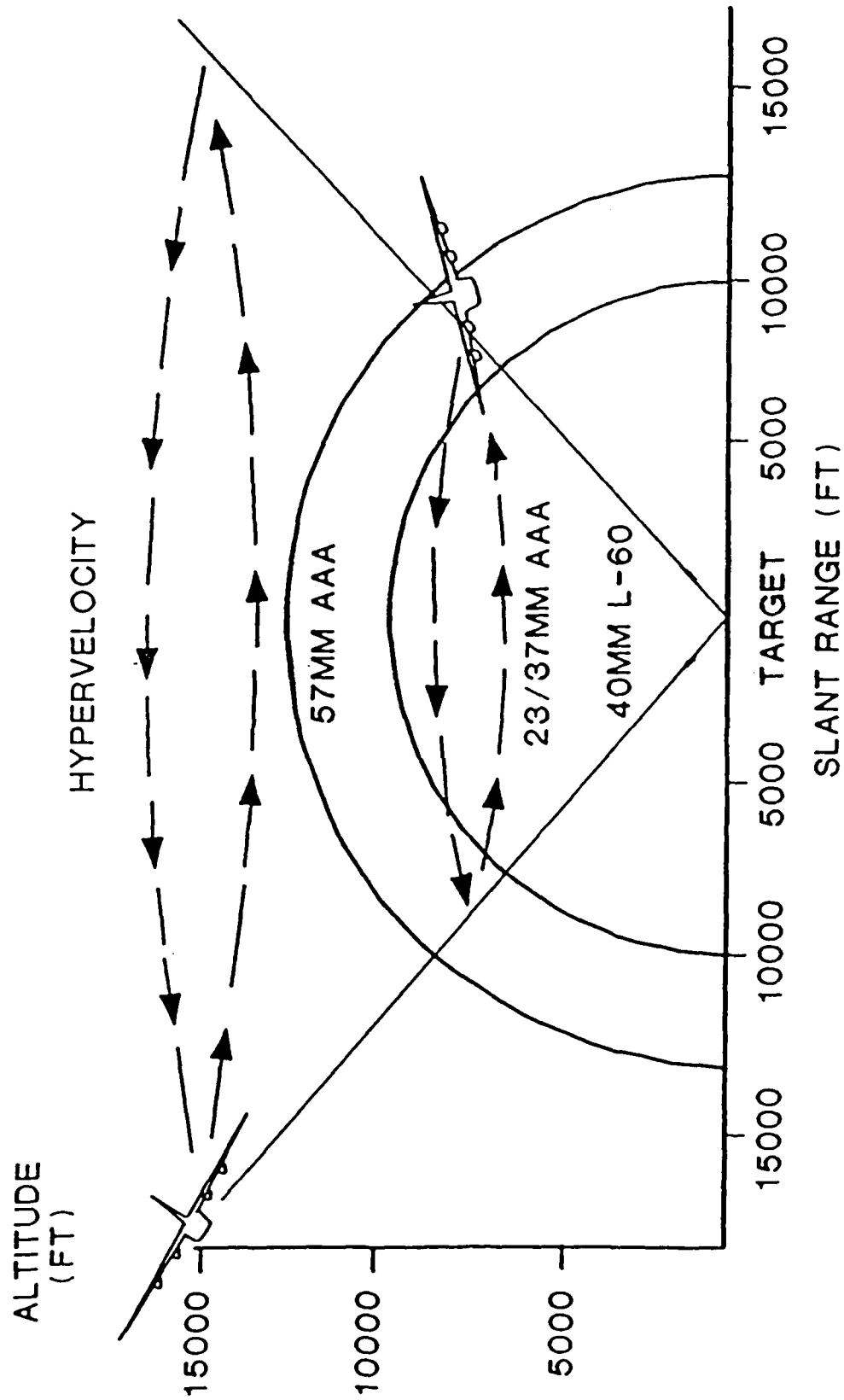
Figure 1. C-130 Gunship performance improvement.

2

Electric guns share advantages such as higher velocities, insensitive munitions, velocity control from round to round and more rounds storable in a given magazine size.

The disadvantages come primarily in the requirement for an electrical power conditioning system and in increased complexity of the complete system. If an electrical power supply is already available, an electric gun may be a convenient add-on to other systems.

There are significant differences between the two main electric gun technologies. Electrothermal gun can use standard gun components and munitions, while rail guns require a split barrel and nonconducting (or insulated) munitions. On the other side, rail guns are theoretically able to achieve higher velocities, because the driving force follows the projectile down the barrel.

Both kinds of electric guns have potential problems with barrel erosion. Control of this erosion will improve the accuracy of the gun and the lifetime of the components.

The objective of this effort is to produce analytic and numerical models of the processes which are related to this erosion and to the performance of the guns. The gas flow along the barrel wall and the heat transport to that wall play a crucial role in these processes.

The following chapters describe in turn the physics of the flow and transport processes, their numerical treatment and the results of computations. These are followed by a chapter drawing conclusions from this year of work.

Physics

Conventional service guns have relatively low velocity capability, but specialized guns have no such limit. So-called "light-gas guns" have achieved velocities over 5 km/sec with kilogram projectiles, and approach 10 km/sec with few-gram projectiles. They are not weaponizable because some components of the breech are destroyed in each shot.

These light-gas guns provide considerable information about the limits of component performance in high-velocity guns. The gas flow in the barrel, and the damage it does to the barrel are not well understood.

The basic flow process is straightforward. A source of mass and energy at the breech end of the gun produces high pressure. This pressure accelerates the propellant material down the barrel, accelerating a projectile.

Two things limit the ultimate speed this projectile can reach. One is the sound speed of the gas. The second is the interaction between the gas flow and the barrel wall.
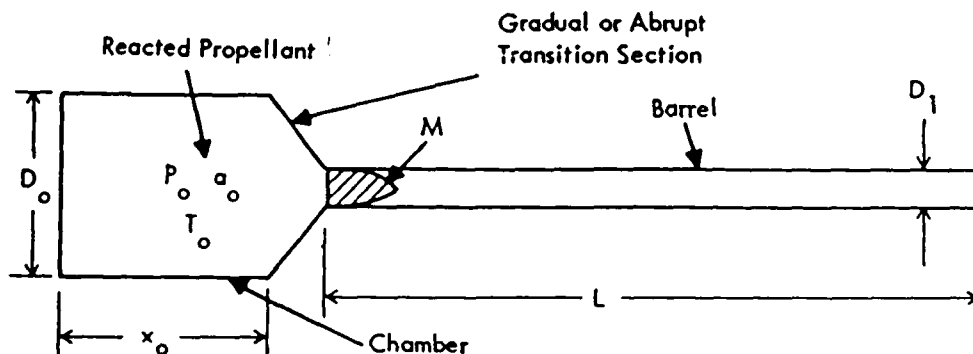

Figure 2. Schematic illustration of conventional gun structure.

4

The effect of the gas sound speed is well known and readily calculable. Figure 2 shows the basic structure of a conventional gun. Reacted propellant of pressure P and temperature T in a chamber reservoir expand through a breech and accelerate a projectile of mass M down a barrel. This process bears a close relation to the operation of an Electrothermal gun, and a more distant relation to the operation of an Electromagnetic gun.

Seigel[1] has calculated the performance of a "Pre-burned Propellant Ideal Gas" (PPIG) gun, and numerically determined the acceleration that can be expected with various gun configurations. His results are in excellent agreement with experiments on chemically driven high-velocity guns such as light-gas guns.

His analysis begins with a simplified version of the equations which are presented in the following section. This is a natural starting place for the analysis of any high-velocity gun. These equations will be used to analyze the dynamics of electric guns.

General equations

The propellant in a conventional gun is obtained as the reaction products of a chemical burn (the PPIG pre-burned propellant). In an electrothermal gun, the propellant is evaporated from fill material in a capillary tube behind the gun breech (Figure 3). This means the pressure and temperature of the propellant are determined by the electrical energy input, rather than simple adiabatic expansion.

RADIATION FLUX

PLASMA JET

PS S

INSULATOR

CONSUMABLE
PLASTIC OR LIQUID
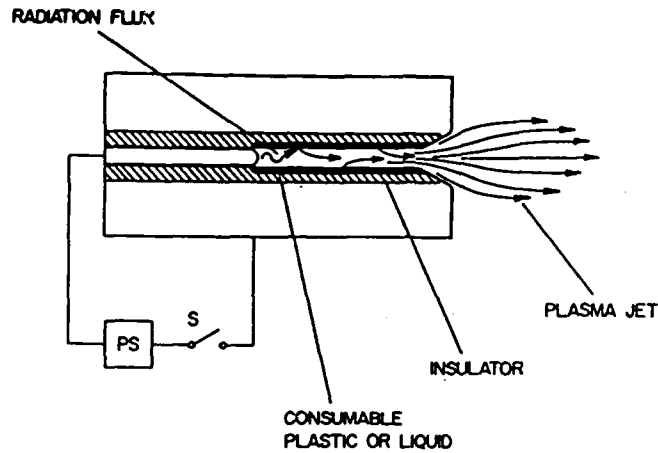
Figure 3. Electrothermal gun capillary structure.

In an electromagnetic gun, the propellant is composed of armature and barrel material ablated by the armature arc. The electrical energy is deposited near the projectile rather than at the breech, but the force is still transmitted to the projectile by propellant pressure.

In general, gun material is converted to propelling fluid and compressed by thermal or magnetic forces. The propelling fluid satisfies the continuity equation

$$\frac{d\rho}{dt} + \rho \, \underline{\nabla} \cdot \underline{v} = \frac{\delta\rho}{\delta t} \qquad , \tag{3.1}$$

where $\delta\rho/\delta t$ is the rate of ablation or evaporation of propelling fluid. In the barrel, the wall ablates, creating the erosion problem that limits barrel lifetime. In addition to fluid production, pressure gradients and viscous stress affect the fluid flow velocity

$$\rho \, \frac{d\underline{v}}{dt} = J \times B - \underline{\nabla} P - \underline{\nabla} \cdot \underline{\underline{\pi}} \tag{3.2}$$

and, in conjunction with other transport processes, they determine the evolution of the fluid total energy

$$\frac{dE}{dt} + E \, \underline{\nabla} \cdot \underline{v} = \frac{\partial P}{\partial t} - \underline{\nabla} \cdot (\pi \cdot v) + W - Q \qquad , \qquad (3.3)$$

where

$$E = \tfrac{1}{2} \rho V^2 + U + P \qquad ,$$

and U is the fluid internal energy. The heat input is by Ohmic heating where current flows in the fluid

$$W = \eta \, J^2$$

and the heat transfer and loss terms considered here are thermal conduction and radiation

$$Q = - \underline{\nabla} \cdot K_H \underline{\nabla} T - \underline{\nabla} \cdot K_R \underline{\nabla} T$$

and turbulence. The turbulence has been examined in detail analytically.[2] These studies have shown that the effects of small eddies can be approximated by a term with the same functional dependence as the bulk viscosity. The result of such an inclusion is the production of larger-scale eddies which are very similar to those which are produced by conventional turbulent mixing in the boundary layer.

These equations describe the dynamics of the propelling fluid flow, but they must be supplemented by information about the properties of the fluid itself. This information is provided by the equation of state. We will use it in the form

$$T = T(\rho, U) \qquad (3.4)$$

$$P = P(\rho, U)$$

After specifying these quantities, the mathematical problem is complete when the transport coefficients are specified.

7

Transport processes

The fluid heating, W, in both the ET and EM case is by electrical Ohmic heating. The plasma has a resistivity[3]

$$\eta = \eta_0 \; Z\ell n\Lambda(1 + 2 \; \nu_{eo} \; /\nu_{ei})/\pi T^{3/2} \tag{3.5}$$

The location of the heating is different in the two cases and will be discussed in the following sections.

The viscosity is a symmetric tensor proportional to the velocity shear with geometric adjustments for divergent flow[4]

$$\pi_{\alpha\beta} = - K_T \left[\frac{\partial V\alpha}{\partial x\beta} + \frac{\partial V\beta}{\partial x\alpha} - \frac{2}{3} \delta\alpha\beta \; \underline{\nabla} \cdot \underline{v} \right] \tag{3.6}$$

with a coefficient that in weak magnetic fields or high density is a strong function of temperature and a weak function of density[5]

$$K_T = 0.42 \; \frac{\sqrt{m} \; (KT)^{5/2}}{e^4 \; \ell n \; \Lambda} \tag{3.7}$$

Its effect on the energetics of the flow is to convert kinetic energy to thermal energy in regions of sheared flow.

In regions with substantial Ohmic heating, the central bore temperature goes well above the melting point of the wall, and the boundary layer is subject to heat transport by both conduction and radiation. The radiation transport is a complex non-local process, but in the black-body case it can be modeled by a diffusion coefficient

$$q_R = - K_R \nabla T \tag{3.8}$$

8

where K_R is the Rosseland mean opacity. It is tabulated in the Los Alamos National Laboratories SESAME Tables.[8]

Electrothermal case

An electrothermal gun is a natural extension of classical gun technology. It uses conventional gun barrels and projectiles. The new advance comes from replacing the chemical propellant with a combination of a propelling medium of choice and electrical energy.

Figure 4 is an illustration of an electrothermal (ET) gun. Electric energy is delivered to the gun by a power conditioning system that shapes the electrical power pulse as needed for gun operation. A cartridge confines an electrical arc which converts the power into heat, pressurizing the propelling fluid.

After the electrical energy has been delivered to it, the gun behaves like a conventional powder gun, with the propellant chasing the projectile down a conventional metal barrel. The ET gun greatly outperforms a chemical gun for two reasons:

1. The propelling fluid may be chosen to have better fluid properties than chemical propellants, since it is not restricted to exothermal materials. In particular, it can be a low molecular weight material, to produce a high sound speed and therefore a propelling fluid which can transmit pressure down the barrel at high speeds.
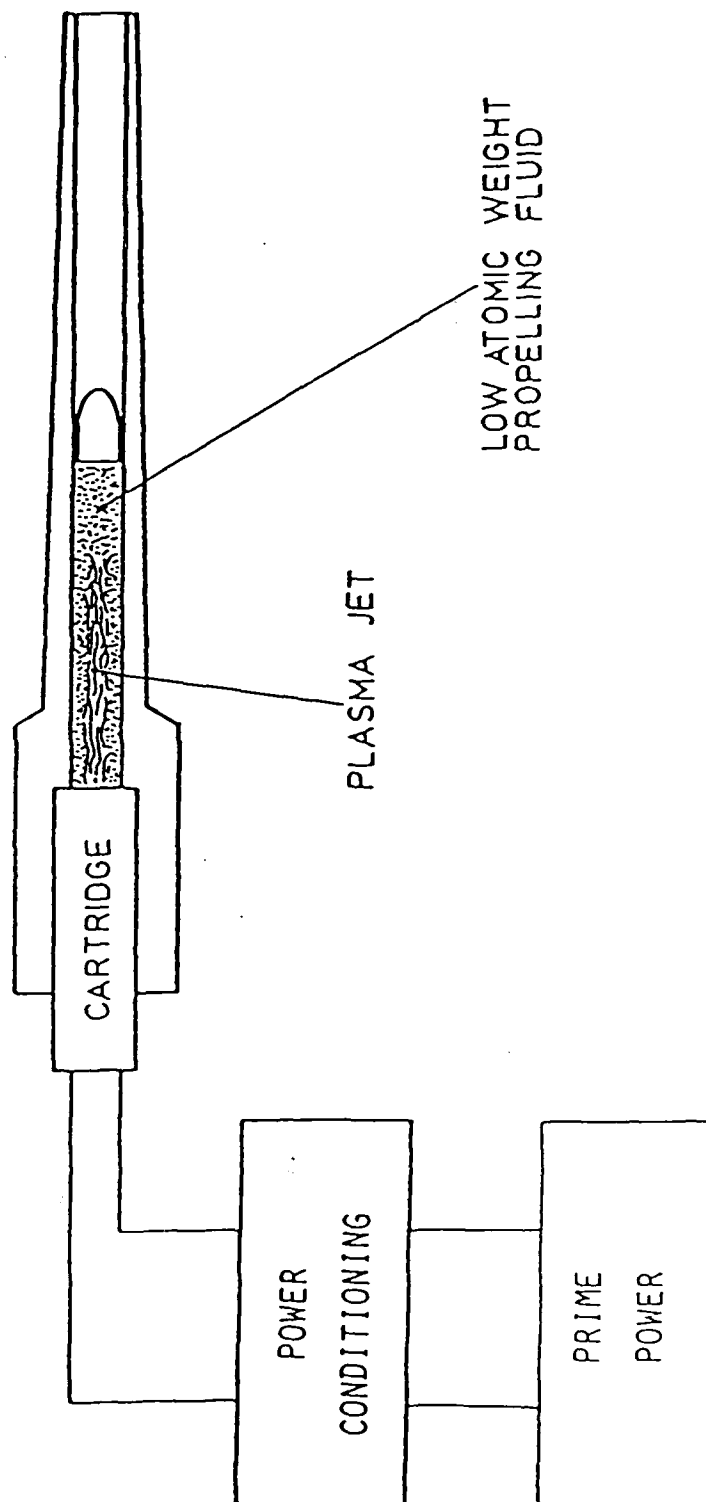
Figure 4. Illustration of Electrothermal gun structure.

LOW ATOMIC WEIGHT PROPELLING FLUID

PLASMA JET

CARTRIDGE

POWER CONDITIONING

PRIME POWER

10

2. The electrical power pulse can be shaped to maintain high pressure throughout the projectile acceleration down the barrel. This is in contrast to chemical burn, which usually produces a rapid rise to peak pressure before the projectile has had much opportunity to move, followed by a decaying pressure as the projectile accelerates. The ET power input can be programmed to produce a constant pressure near the maximum pressure the gun can withstand.

Figure 5 compares the theoretical and measured performance of the ET gun with conventional guns. The ET gun can reach speeds unavailable to conventional guns, and do reach comparable velocities with much higher efficiency.

The ET gun also has problems which must be considered. The principal one is that the high temperatures in the cartridge, and the high flow velocities can easily erode and damage the gun bore. Powder guns also have a bore erosion problem, but they also have many years of design and development devoted to its management. The present effort has aided similar developments for the electrothermal gun.

The energy is delivered to the ET gun by Ohmic heating in the cartridge. In this region, the temperatures reach typically 40,000°K, and the surface of solids rapidly evaporates. The densities are high enough that the radiation takes on black-body form and the central temperature becomes

$$T(eV) = 1.8 \left\{ \left(\frac{I}{10^5} \right)^4 \left[\frac{Z \ln \Lambda}{a^3} \left(1 + 2 \nu_{eo} / \nu_{ei} \right) \right]^2 \right\}^{1/11} \qquad (3.9)$$

This relation is obtained from steady-state equations for the heat deposition and transport in the cartridge.
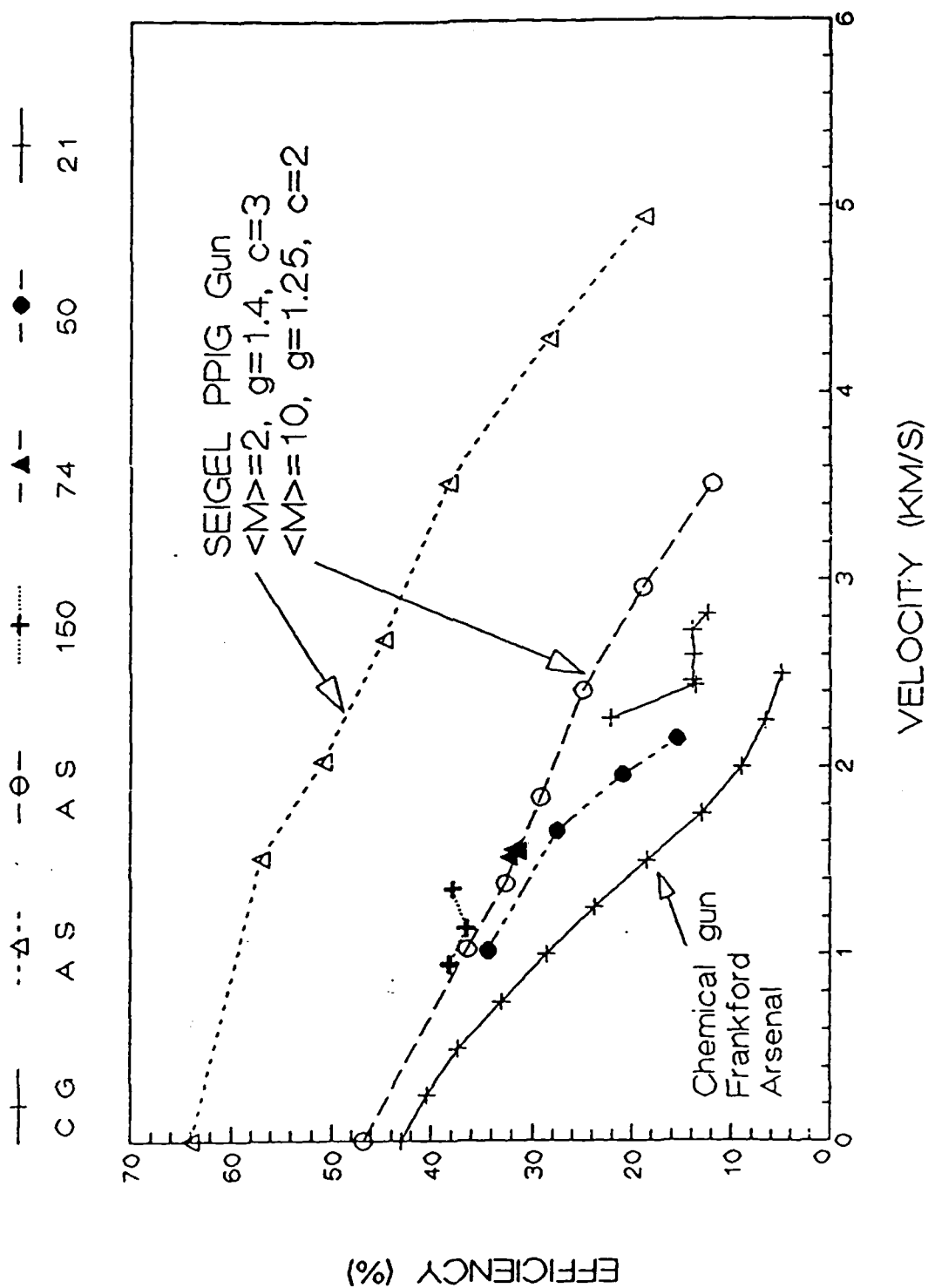
Figure 5. Performance of Electrothermal and conventional guns.

Figure 6 schematically indicates the shape of this layer, and the competing transport processes which determine the shape and width of the layer. Because of the very steep gradients in this sheath, the transport to the wall takes place on a much shorter time scale than the axial transport. This allows the radial transport to be treated asymptotically in the axial transport calculations.

Figure 6. Thermal transport skin layer in a gun bore.

13

Electromagnetic case

An electromagnetic (EM) gun is depicted schematically in Figure 7. Like the ET gun, the electric energy is delivered at the breech of the gun (or, in more complicated arrangements, at a number of feed points along the bore). Unlike the ET gun, the EM gun deposits electrical energy close to the projectile, with the deposition region traveling along the bore with it.
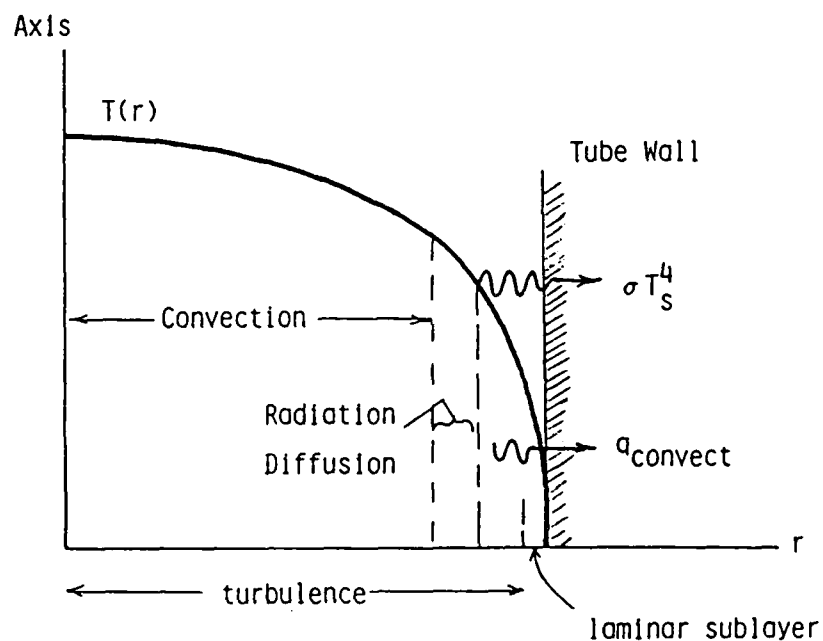
The bore is split, consisting of two rails and two insulators, usually arranged in a circular or square cross-section. It is normally under external compression, at least to the peak pressure anticipated during gun operation.

The energy deposition region within the bore is called an "armature" in analogy to the armature on a motor, where current is transferred from a stationary conductor to a moving conductor. In the 1970's, solid armatures were tried, but it was found that a thin plasma formed between the solid and the rails, and damaged the rails. The damage could be reduced by increasing the size (and mass) of the armature, but that reduced the useful projectile payload. As a result, most high-velocity railguns now use plasma armatures, both to reduce the armature mass and to increase the area of the armature, thus hopefully spreading out the heat load on the bore.

In the EM gun, the current flows from one rail to the other. In this geometry, the resistance is

$$R = \eta_0 \; Z \; \ell n\Lambda \; (1 + 2 \; \nu_{eo} / \nu_{ei}) \; G/x_A T^{3/2} \qquad (3.10)$$

where x_A is the armature length and the geometry is characterized by the factor $G = 1$ for a square bore, and $G = \Pi/4$ for circular bore. For a constant-mass armature with sound speed c_s, the armature length is
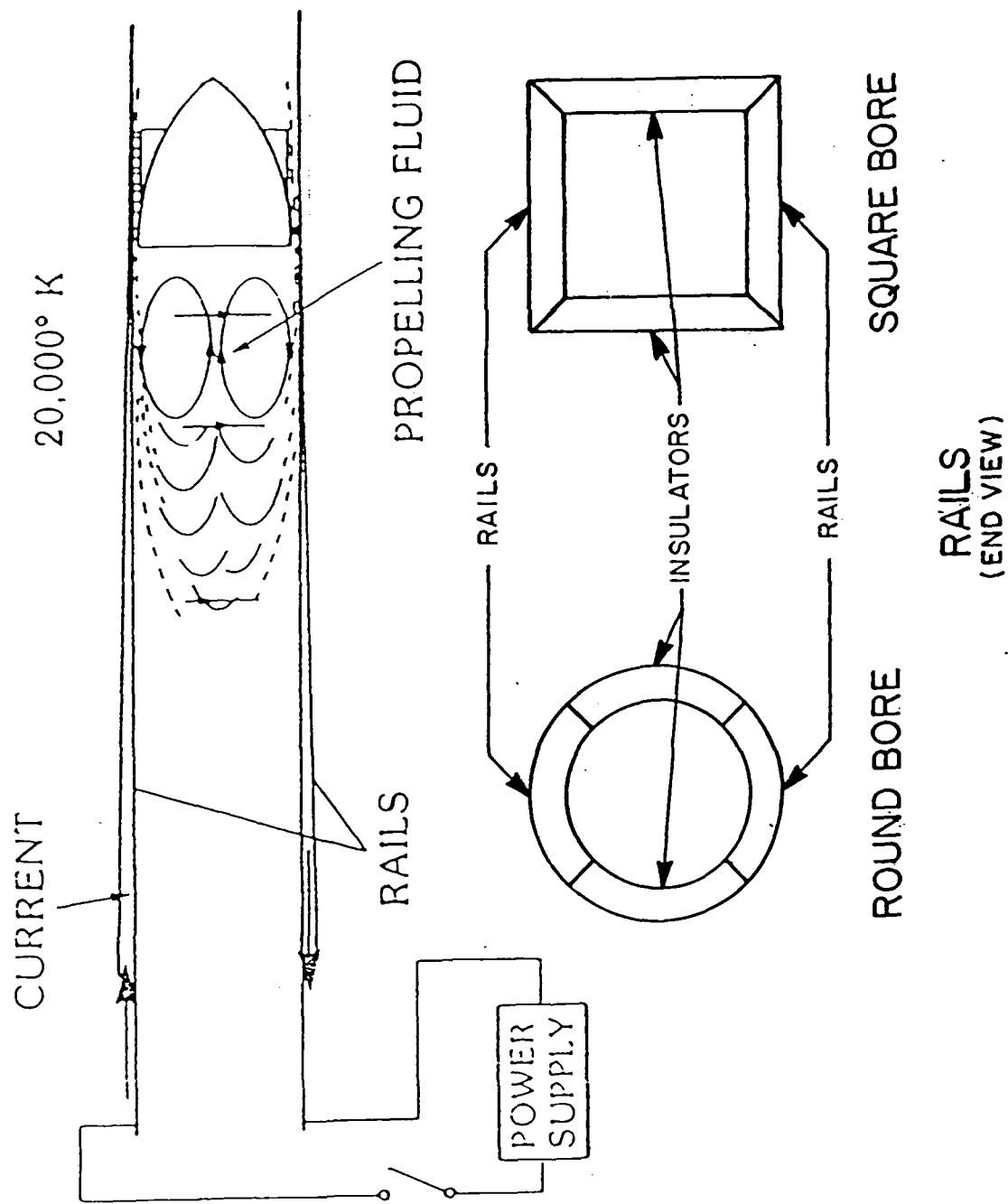
14

Figure 7. Structure of an Electromagnetic (rail) gun.

15

$$x_A = AC_s^2 / \Upsilon M_A P \qquad\qquad (3.11)$$

where A is the cross-sectional area of the bore, and Υ and M_A are the armature adiabatic constant and mass, respectively.

The propelling fluid in the EM gun may start out as some fuse or other selected material, but it usually quickly becomes dominated by rail and insulator material. The bore wall is subjected to the very high temperatures of the armature plasma. As the armature moves down the bore, it evaporates wall material, which may be swept up in the armature arc and carried along with the projectile. This mix of materials is the armature fluid.

The primary focus of this research effort is the flow and operation of the electrothermal gun. However, the models which have been developed retain sufficient generality to treat the electromagnetic gun with appropriate changes in the resistivity and geometry.

Numerics

The equations presented in the previous section are both complex and nonlinear. Some progress can be made in their solution analytically, but many approximations are required.

Numerical calculation of the solutions has the advantage that accurate results can be obtained without these approximations. It has the disadvantage that, for nonlinear equations, a numerical solution applies only for the specific case calculated, and not for a class of solutions, as can be obtained with analytic scaling laws.

On the other hand, numerical results can often lead to empirical relations which are very useful, and can verify the accuracy of analytic results which are obtained via approximations whose validity is otherwise hard to assess.

This section takes the equations from the previous section, converts them to forms which are more conveniently handled numerically, and sketches how they are solved numerically. This provides the framework within which the transport research and electric gun development is carried out.

Conservation laws

Numerical simulation of fluid flow in the gun bore has the advantage that it can treat non-linearities and functional dependencies without approximation. It has the disadvantage that it makes other approximations to treat a problem with practically infinite degrees of freedom. One way or another, it reduces the problem to a finite number of degrees of freedom.

The method used here is finite-difference formulation of the numerical problem. The continuous variables of the problem are replaced by a finite number of discrete values, arrayed along coordinate axes. It is then desirable to express the equations in a way which preserves the physics of the problem as well as possible, given the necessity for this discretization.

One effective method is to cast the equations to be solved in conservation-law form. This is easy for the mass, momentum and energy equations. Then a numerical method can be used which preserves this conservation property to the maximum accuracy available on the computer of choice.

This is how we proceed here.

The mass transport equation (3.1) can be converted to conservation-law form by rewriting its total time derivative as a partial time derivative plus a convective derivative and collecting terms

$$\frac{\partial \rho}{\partial t} + \underline{\nabla} \cdot \rho \underline{v} = \frac{\delta \rho}{\delta t} \tag{4.1}$$

Multiplying this equation by $\underline{v}$ and subtracting it from Eq. (3.2) yields the conservation-law form of the momentum equation

$$\frac{\partial}{\partial t} (\rho \underline{v}) + \underline{\nabla} \cdot (\rho \underline{v} \, \underline{v}) = J \times B - \underline{\nabla}P - \underline{\nabla} \cdot \underline{\underline{\pi}} \tag{4.2}$$

A similar manipulation converts the energy equation to

$$\frac{\partial E}{\partial t} + \underline{\nabla} \cdot E\underline{u} = \frac{\partial P}{\partial t} - \nabla \cdot (\underline{\underline{\pi}} \cdot v) + W - Q \tag{4.3}$$

The remainder of the equations in Section 3 are scalar, and do not require further manipulation.

Finite-difference formulation

The simplest view of the finite difference formulation of these differential equations can be illustrated by expressing the derivatives in Eq. (4.1) in terms of values of the variable on a discrete one-dimensional mesh. That is,

$$\nabla \cdot \rho v = \left(\rho_{i+1} \; V_{i+1} - \rho_i \; V_i \right) \Big/ \left(X_{i+1} - X_i \right) + 0 \left(X_{i+1} - X_i \right)^2 \quad (4.4)$$

where the subscript i refers to the value of the variable at the location x_i. By the mean value theorem, this is the exact value of the derivative at some point between x_i and x_{i+1}. The most probable location is the midpoint

$$X_{i+\frac{1}{2}} = \tfrac{1}{2}\left(X_{i+1} + X_i \right) \quad (4.5)$$

The next step in a finite-difference formulation is discretizing the time. In terms of a time-step δt, the mass conservation equation becomes

$$\left(\rho^{(t+\delta t)} - \rho^{(t)} \right) \Big/ \delta t + \left(\rho_{i+1} V_{i+1} - \rho_i V_i \right) \Big/ \left(X_{i+1} - X_i \right) = \frac{\delta \rho}{\delta t} \quad (4.6)$$

Again, the "centering" of the time values is important. With centered differences in both time and space, this equation is

$$\left(\rho_{i+\frac{1}{2}}^{(t+\delta t)} - \rho_{i+\frac{1}{2}}^{(t)} \right) \Big/ \delta t + \left(\rho_{i+1}^{(t+\frac{1}{2}\delta t)} V_{i+1}^{(t+\frac{1}{2}\delta t)} - \rho_i^{(t+\frac{1}{2}\delta t)} V_i^{(t+\frac{1}{2}\delta t)} \right) \Big/ (X_{i+1} - X_i) = \frac{\delta \rho}{\delta t} \quad (4.7)$$

This result is the simplest second-order accurate finite-difference formulation of Eq. (3.1). It is called a "leap-frog" algorithm because the density leaps from time $t-\delta t/2$ to $t+\delta t/2$ over the values of density and velocity at time t.

One major problem with using a formulation such as this is that the values of density and velocity must be determined at

19

different times and locations, and unless great care is taken at keeping them synchronized, these different grids can drift apart, yielding nonphysical results.

For this reason it is prudent to use a numerical algorithm which has been thoroughly tested and designed for the kind of solutions one expects from the equations. The Flux-Corrected Transport algorithm is chosen for this case.

Flux-corrected transport

The propelling fluid in the gun bore has a number of properties that can make numerical treatment difficult. It has steep gradients near the boundaries. The electrical discharge can produce rapid time rates of change, causing dynamic steep gradients, perhaps leading to shock waves.

Flux-Corrected Transport is an algorithm which was developed with such applications in mind. Figure 8 compares it with leapfrog and two other popular algorithms in the propagation of a very steep (square) density wave.

FCT begins with a second-order accurate time-advance algorithm, and extends it by examining the flux at each grid point to insure that certain physically-derived inequalities are satisfied. (These inequalities are violated by many popular numerical algorithms when steep gradients or shock behavior is obtained in the solution. The result of the violation is non-physical oscillatory behavior of the numerical solutions.)

The FCT algorithm was published in the form of a FORTRAN program. It is used here with minor variations on the published form.
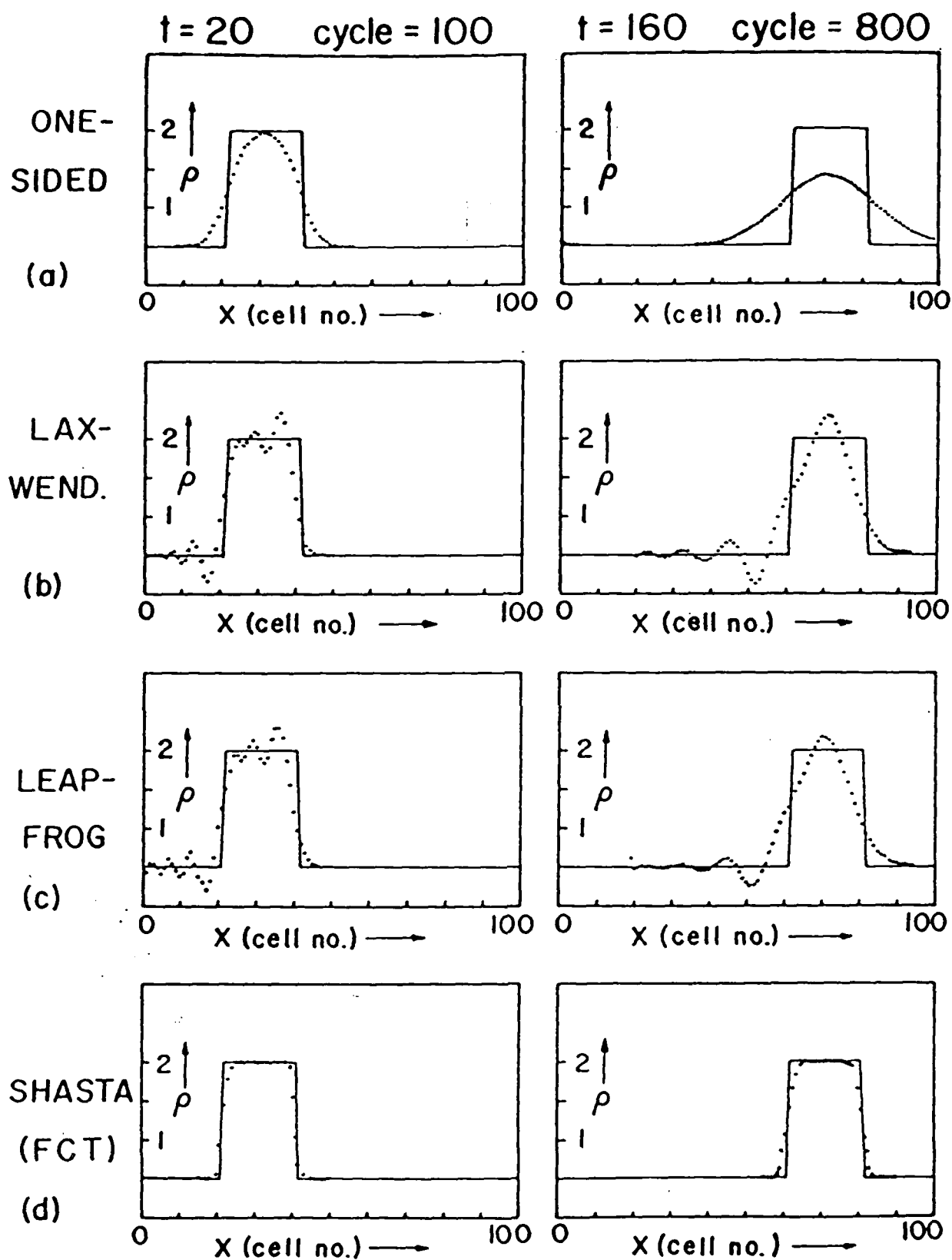
20

t = 20   cycle = 100   t = 160   cycle = 800

ONE-SIDED (a)

LAX-WEND. (b)

LEAP-FROG (c)

SHASTA (FCT) (d)

Figure 8. Comparison of several numerical algorithms.

21

The FCT algorithm assumes that the equations have been cast in conservation-law form, and calculates the time-advance of each conserved quantity, given the right-hand side, or "source" terms. That is, FCT is formulated principally as a Fortran subroutine which accepts as input vectors of conserved quantities and source terms, and produces as output the vector at a future time.

One very important feature of FCT is that it makes use of all quantities, both variables and sources, at the same time and space positions, avoiding the problem described above in terms of the leapfrog algorithm.

In order to obtain optimum performance from FCT, and to preserve second-order accuracy in time, it is used in a predictor-corrector formulation. That is, FCT calls are first made to advance each of Eqs. (4.1-4.3) a time $\frac{1}{2}\delta t$. Then the sources are evaluated and a second series of calls is made to advance the physical variables to the full time step, δt.

Computation and experiment

For electric guns, both modeling and experiment have advanced substantially during this year. Modifications of Electrothermal guns have allowed operation with virtually ablation-free barrels. In Electromagnetic guns, the thermal behavior of the conducting rails and the insulators has been characterized, leading to a more complete understanding of how to operate within the limitations of the materials.

The computer model has been written in a general form to allow calculations for both kinds of guns. It is organized with distinct physical processes in separate subroutines. Each subroutine has a specific function, divided by physical or computational processes, such as electrical heating, fluid properties, acceleration, transport, diagnostics and output.

Each subroutine has multiple entries. The different entries in each subroutine perform parallel functions, such as initialization, data entry, parameter evaluation, output and termination. Compared with the use of subroutines without entries, the use of multiple entries reduces the use of COMMON statements for the variables.

Nevertheless, most of the key variables are stored in COMMON blocks. These blocks are named, and entered into the subroutines that use them by INCLUDE statements. This prevents misspellings or similar problems which could put the COMMON variables at different locations in different subroutines.

Program structure

The program is written in FORTRAN for the Digital Equipment Corporation VAX computer series. Because the VAX is a minicomputer, some compromises must be made in the program design.

For convenient access to the source, it is desirable to have the program in a single file. This allows such convenient operations as global search, global replace, block moves and other editing practices which are more conveniently done on a single file.

On the other hand, a model of this size takes a long time to develop, and a long time to completely recompile after a change has been made. For this reason, separate modules might be preferred, so that when only one or a few have been changed, only those few must be recompiled and linked.

To make both of these approaches possible, the program was structured so that both options were available. A command file was built containing the source routines, separated by CREATE commands. The created files have alphabetically ordered names so that the contained subroutines can be found in the same order in the VAX directory.

When complete recompilation is desired, the command file is executed, splitting the complete source into a number of files, compiling all of them and storing the object files in a library. The smaller source files are then available for change and rapid recompilation.

In this way, the complete executable file can be built from individually recompiled files and the object modules which are stored in the library. This speeds development when small parts

of the program are changed and global operations are not required.

Electrothermal results

Heat flow to the wall of a gun barrel has been studied empirically for many years. More recently, progress has been made in analytically determining the importance of various factors in the process.[6]

For the Electrothermal gun, one main objective of heat transport analysis is to identify the conditions under which the gun can be operated without erosion of the gun bore. The thermal skin in which all the heat transport processes are competing is the key to understanding the physics of this process.

Figure 6 illustrates the interplay of the major processes in the transport. Radiation carries energy toward the wall. As transport to the wall begins to cool the edge of the propelling gas flow, the black-body transport gives way to radiation diffusion, and finally direct radiation to the wall. Radiation is competing in the thermal sublayer with direct thermal conduction and turbulent convection, both of which become progressively more rapid as the temperature gradient becomes steeper at the bore wall.

The response of the wall to the heat load from the flowing propellant is described by a heat flow equation for the metal of the barrel. It is

$$\rho_w C_v \frac{\partial T}{\partial t} - K_T \frac{\partial^2 T}{\partial x^2} = q_w \qquad (5.1)$$

25

where $T(x,t)$ is the wall surface temperature, ρ_W is the wall mass density, C_v is its heat capacity, q_w is the heat load on the wall and K_v is its thermal conductivity. The solution of this equation requires advanced methods, such as Green's functions[7] or asymptotic expansion of the Riemann function.[8] The key result is that the homogeneous solution (for $q_w = 0$) of Eq. (5.1) is

$$T_H = \frac{\rho_W C_v}{\pi k_T t} \, e^{-\frac{K_T X^2}{4\rho_W C_v t}} \tag{5.2}$$

The particular solution for this problem can then be obtained by writing $T = T_H(x,t)F(t)$, and noting that conservation of energy requires

$$\int_\partial^\infty \rho_W c_v \, T \, dx = q_w t \tag{5.3}$$

For a constant heat load, the wall temperature rise obeys the equation

$$\Delta Tw = \frac{2 \, q_w \sqrt{t}}{\sqrt{\pi \rho_W c_v k_T}} \equiv f \, q_w \, \sqrt{t} \tag{5.4}$$

and the temperature rises at a rate proportional to $t^{\frac{1}{2}}$. The actual rate depends on the material properties, in a way which helps select among various candidate wall materials.

A metal which is a good candidate for the bore surface of gun barrel should have a large heat capacity, a large thermal conductivity and a high melting point. The merits of these characteristics can be quantified in the performance factor, f, defined in Equation (5.4). The quantity f becomes larger for a wall material which is more resistant to heat damage. Table 1 presents experimental values of key transport parameters and computed performance data for various barrel conductors.

Material	Cu–Al$_2$O$_3$	Mo–Ti–Zr	W–Ni–Cu	W–Ni–Fe	W–Ni–Fe–Cu
Trade Name	Glidcop AL–15	TZM	HD–17	X–5	X–11
Density x10^3 Kg/m^3	8.8	9.0	17	18.4	18.5
Specific Heat x10^3 J/Kg–$^\circ$K	0.50	0.30	0.16	0.14	0.15
Yield Strength MPa	320	380	90	120	120
Young's Modulus GPa	120	320	280	350	350
Thermal Cond. x100 W/m–$^\circ$K	3.2	1.0	0.94	0.88	0.88
Electrical Conduct. % IACS	92	32	14	13	13
Working Temp. $^\circ$K	1260	1920	1300	1300	1300
Melting Temp. $^\circ$K	1356	1998	1356	1623	1356
Evap. Temp. $^\circ$K	2868	5833	6203	6203	6203
Perf. Factor (f) x10^4 m^2–$^\circ$K/W s	0.30	0.69	0.70	0.75	0.72
Work Limit $(T_w-T_0)/f$	3.2	2.4	1.4	1.3	1.4
Melt Limit $(T_M-T_0)/f$	3.5	2.5	1.7	1.8	1.5
Evap Limit $(T_E-T_0)/f$	8.6	8.0	8.4	7.9	8.2

Table 1. Experimental and computed data for high-temperature metal alloys suitable for gun barrels and rails.

The first two materials are low-density highly-conductive materials appropriate for electromagnetic gun rails. The last three, which are sintered materials, have higher density and lower electrical conductivity, and may be appropriate either for a segmented rail gun or for a liner in an electrothermal gun.

The material properties and transport coefficients are needed to determine the behavior of the gun bore under the heat load and stresses delivered to it. The most important properties for the thermal loads are the working, melting and vaporization temperatures.

The computed performance factor (f) determines the ability of the material to withstand the calculated heat load from the interior plasma. This factor, in conjunction with the three critical temperatures, gives figures of merit for the candidate materials under progressively more severe conditions.

The figures of merit are summarized in the Working, Melting and Vaporization limit factors for each material. They show that these materials may soften and flow, but a very large heat input is required to evaporate them and contaminate the propelling plasma. This confirms that these are good choices for gun bore materials.

Table 2 presents comparable data for selected electrical insulators. These materials are necessary in a rail gun in order to electrically isolate the rails. Unfortunately, these electrical insulators are also exposed to the propellant, because they and the rails must share the inner surface of the gun bore.

Material	alpha-SiC	Si_3N_4	B-N	SiO_2	Al_2O_3
Density x10^3 Kg/m^3	3.1	3.2	2.0	2.2	3.6
Specific Heat x10^3 J/Kg-^{o}K	1.3	1.2	2.3	1.2	1.2
Flexural Strength MPa	310	700	47	80	138
Young's Modulus GPa	410	290	80	70	280
Compressive Strength MPa	5160	3500	105	1120	345
Thermal Cond. x100 W/m-^{o}K	0.30	0.18	0.29	0.05	0.06
Working Temp. ^{o}K	2600	1573	2073	1926	2273
Melting Temp. ^{o}K	2773	2173	3255	2001	2326
Evap. Temp. ^{o}K	3073	2173	3255	3223	3253
Perf. Factor (f) x10^4 m^2-^{o}K/W s	1.0	1.4	1.0	3.2	2.2
Work Limit $(T_w-T_0)/f$	2.3	0.9	1.8	0.5	0.9
Melt Limit $(T_M-T_0)/f$	2.5	1.3	3.0	0.5	0.9
Evap Limit $(T_E-T_0)/f$	2.8	1.3	3.0	0.9	1.4

Table 2. Experimental and computed data for high-temperature materials for rail-gun electrical insulators.

29

Comparison of the insulator temperature limit factors with those of the conductors makes it clear that the working and melting limits are in the same range, but the insulators are much more easily evaporated. Other, more conventional insulator materials were subjected to this analysis and calculation, but provided much worse performance, so they are not tabulated here. The key results for them are summarized in figures below.

The computed performance of wall material under a heat load is illustrated in Figure 9. The "Scaled Heat Load" is $(T-T_0)/f$, and can be compared directly with the limits in Table 1.

This omits the working-temperature information, but compares the melting point and evaporation point data with the measured experimental mass loss of gun tube liner material. The onset of mass loss, and dramatic increase of mass loss are clearly correlated to the calculated melting and evaporation points.

The analysis and simulation of this process has suggested several ways to reduce the barrel erosion problem. It is possible to add materials to reduce radiation transport in the boundary layer. One might also add ablatable materials to the wall so that the ablation, when it occurs, only removes the coating, not the wall material. Finally, since so much of the heat transport is driven by the fluid temperature, the performance can be improved most directly by lowering the fluid temperature, but not so much that the gun performance is degraded.

The 20 mm Electrothermal gun is now routinely run with the hot fluid emanating from the cartridge cooled by mixing with a low-temperature medium which is placed outside the capillary. The mixed lower-temperature fluid then travels down the barrel, separated from the barrel wall by a very thin sheath layer.

30

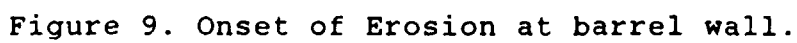Figure 9. Onset of Erosion at barrel wall.

31

Figure 10 schematically illustrates the experimental method which has solved the bore erosion problem for a wide class of Electrothermal gun applications. The solution is the addition of a "mixing chamber" between the capillary, which produces plasmas with temperatures of 30,000 °K to 40,000 °K, and the gun bore, which requires much lower temperatures.

In the upper diagram, the projectile is shown separated from the capillary by a chamber filled with a secondary propellant, such as water or methanol. When electricity is fed to the capillary, the resulting plasma stream must pass through the mixing chamber on its way to the bore.

As depicted in the lower figure, the fluid mixes with the plasma, flowing with it into the bore and accelerating the projectile. In practice, the mixing fluid contains 85-95% of the total propellant mass. This lowers the plasma temperature by more than an order of magnitude, reducing it to temperatures comparable with those in conventional guns.

This method of controlling the propellant temperature allows the heat transport to the barrel to be made comparable with that in conventional guns, while the choice of propellant medium (now primarily the mixing medium), still produces a substantial improvement in gun performance.
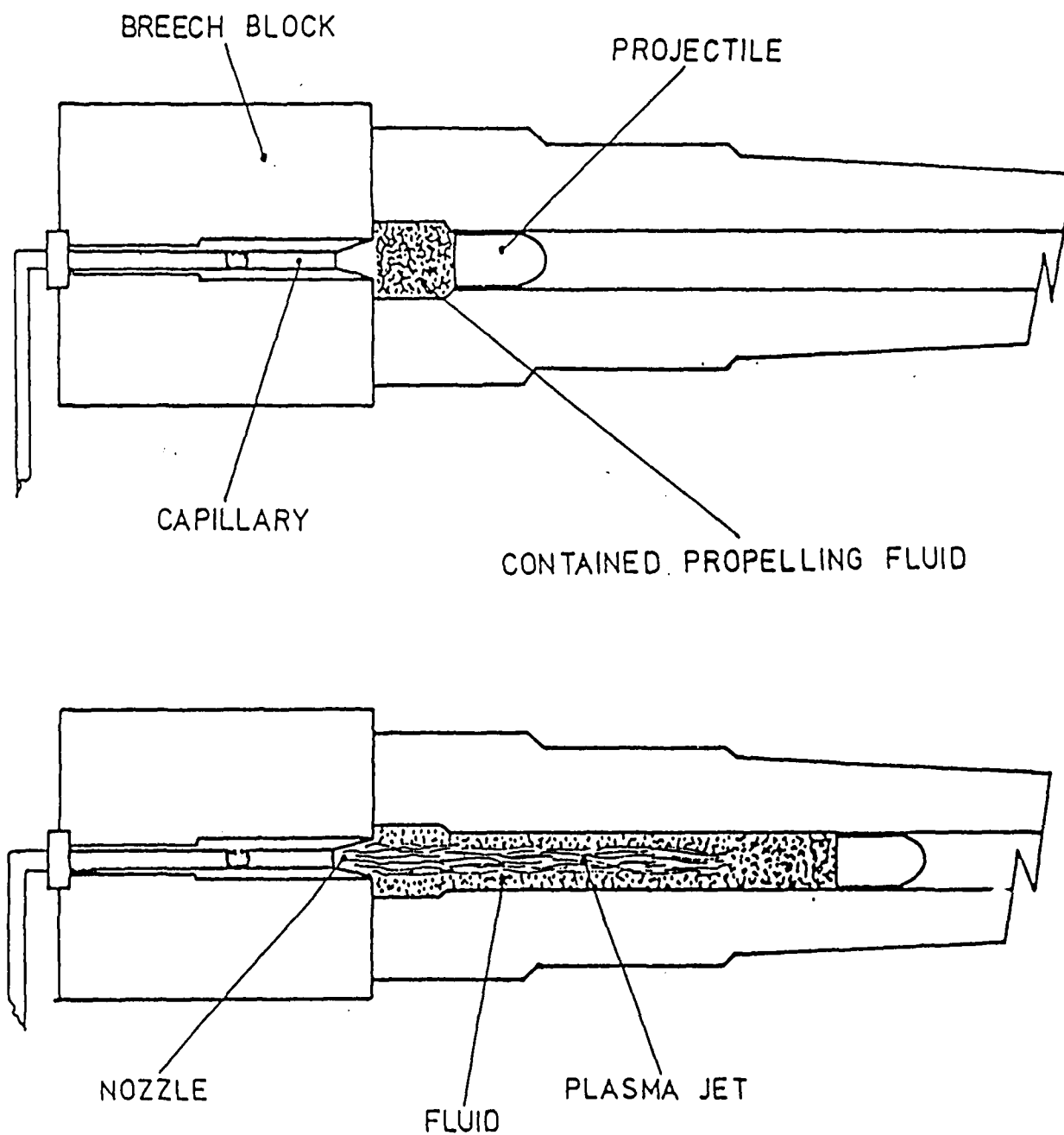
Figure 10. Solution of bore erosion in Electrothermal gun.

33

Electromagnetic Results

The Electromagnetic gun may be thought of as an Electrothermal gun in which the capillary runs after the projectile and pushes directly on it with the aid of electromagnetic forces.

The direct action of the electromagnetic force on the projectile is a clear advantage. It is not necessary to send propellant a long way down a barrel and accept propagation losses before the propellant can deliver energy to the projectile.

On the other hand, electromagnetic radiation ablates everything present in the capillary of an ET gun, and the armature arc in the EM gun is ready and able to do the same ablating in the bore of the EM gun.

The primary heat transport in this case is radiation, since the hot core plasma is well into the black-body regime. The rate at which the energy reaches the wall is then determined by the Rosseland opacity. The best possible case is obtained with Hydrogen, for which the Rosseland opacity is shown in Figure 11. The important thing to note is that this quantity has a very large variation in its values. This means it can be the dominant process in one region, and insignificant nearby.

For the more restricted range of temperatures near the wall, we have developed a bilinear fit in pressure and temperature, so that the complete Sesame tables[9] are not needed. For T > 0.34 eV, the fit is

```
log10(LRoss) =   0.35 - P * 0.35
                -(2.23 - P * 0.16  ) * T
                +(0.58 - P * 0.061 ) * T**2
                -(0.034- P * 0.0062) * T**3
```
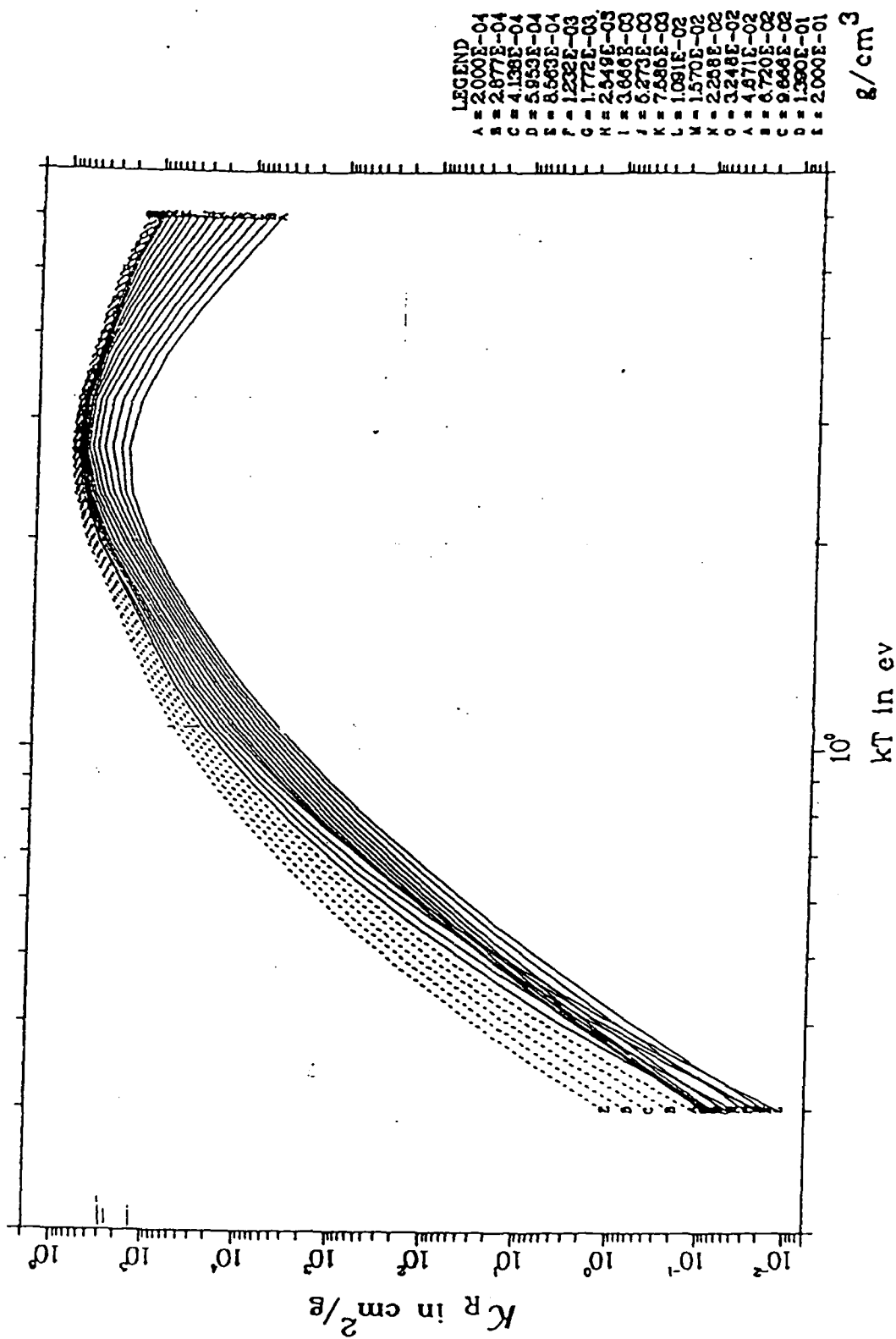
34

Figure 11. Rosseland Opacity of hydrogen versus temperature.

The logarithm is continuous at T = 0.34 eV, and is proportional to 1/T when T < 0.34 eV. This preserves the trends of the Sesame tables without requiring use of the full tables.

Now that the heat load is known, it is appropriate to return to material performance data. Figure 12 shows the mass ablation data for candidate insulator materials. In addition to the materials presented in Table 1, popular rail insulator materials such as Lexan, Vespel, Melamine Glass (G-9), Epoxy glass (G-10) and Polyimide Glass (PI-GL) were evaluated.

Note that the materials of Table 1 are able to tolerate heat load for some time before melting or evaporating, while the composite glasses began to ablate almost immediately. This is why it is important to examine the physical properties and evaluate the performance factor. It is a useful indicator of the suitability of materials for service in electrothermal or electromagnetic gun bores.

Figure 13 combines the results for rail gun conductors and traditional insulators on the same graph. This shows that the problem of insulator ablation is much more severe than rail ablation, when conventional insulating materials are used.

The broken line at 18 milligrams of ablated material is an estimated limit of the maximum tolerable amount of ablation in a small rail gun. Clearly, the conventional insulators have exceeded this limit before any high-performance rails have shown any significant erosion.
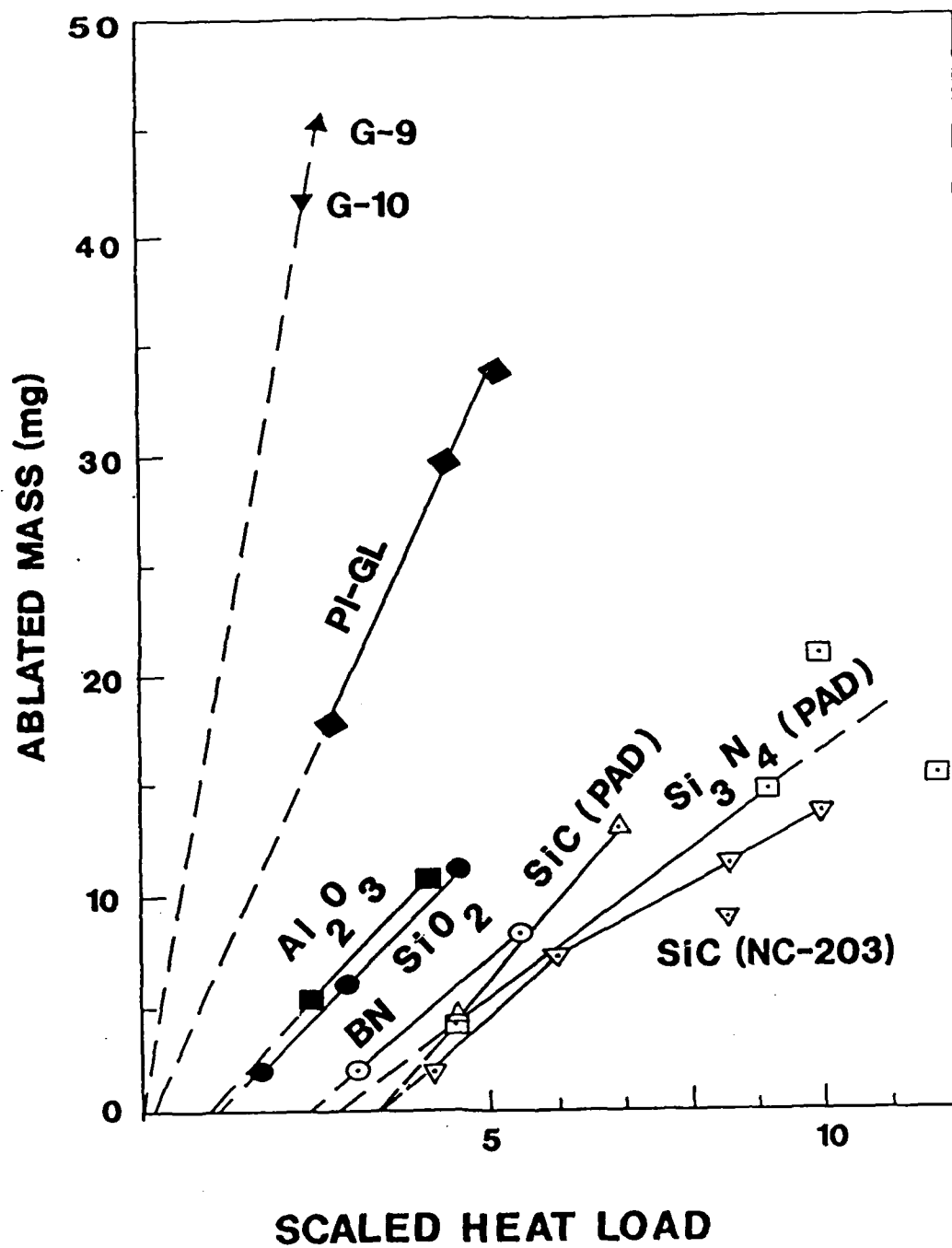
36

Figure 12. Thermal performance of rail gun electrical insulators.

37

The only insulators that have any significant chance of surviving in EM service are Boron Nitride, Silicon Nitride and alpha Silicon Carbide. These materials are difficult to form into appropriate shapes for railgun insulators, but there are possible designs if the overall gun geometry is properly chosen.

The fundamental conclusion is that the conventional Electromagnetic gun will operate with substantial ablation of both rails and insulators under normal conditions. These materials must be considered as the constituents of the armature after the projectile has begun to move, and also as parasitic mass that the projectile must carry with it as it accelerates down the bore.
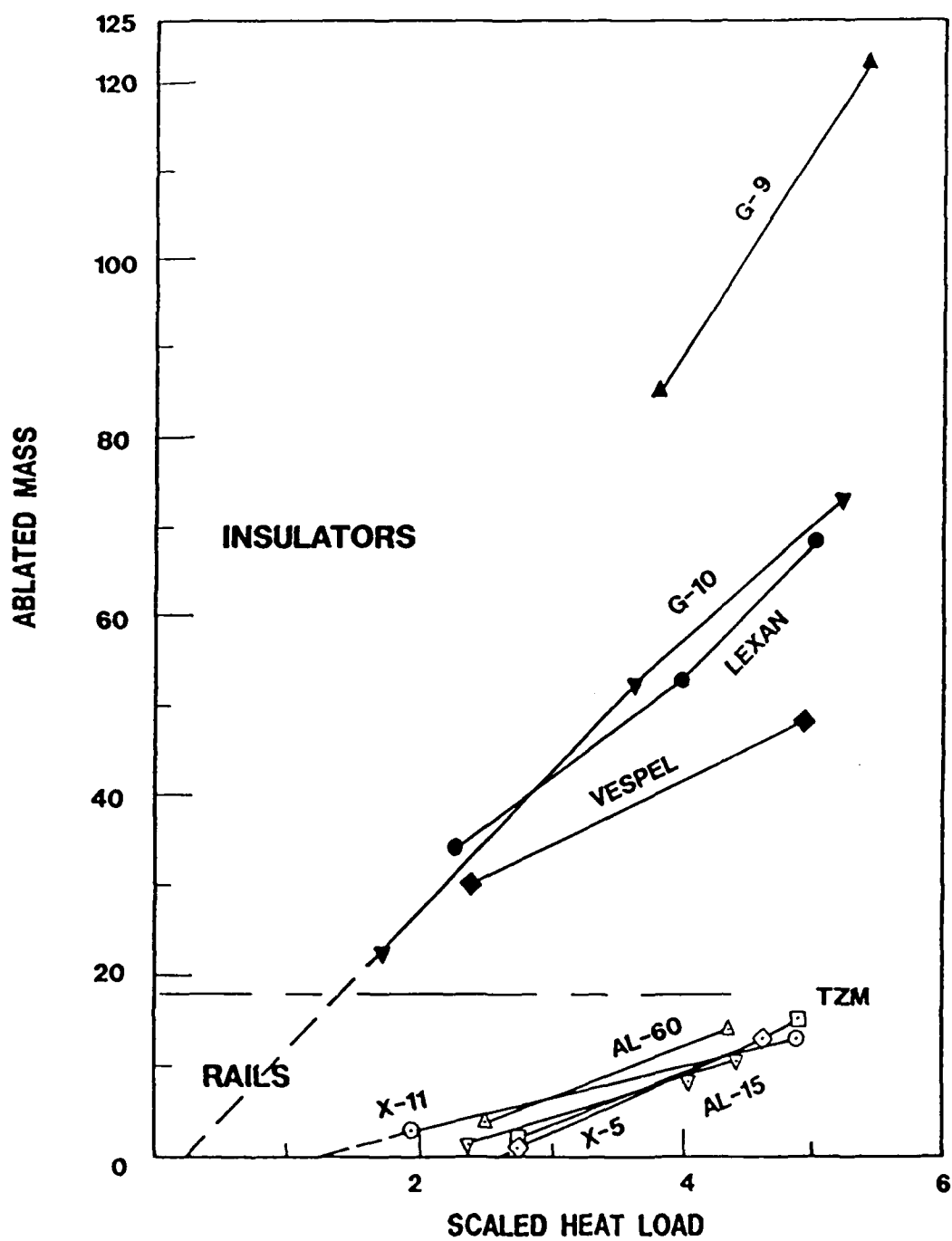
Figure 13. Composite rail and insulator performance.

Conclusions

Radiation, thermal conduction and viscosity and turbulent convection all provide important transport mechanisms in the plasma flow in electric guns. The flow behind a projectile travels at a velocity near the speed of sound, and is separated from the wall by a very thin boundary layer.

The heat transport through this boundary layer is capable of ablating material from the wall, causing erosion which damages the gun bore and reducing the performance of the gun. The amount of damage this transport will do depends on the temperature and flow momentum.

In the Electrothermal gun, study of this transport problem has led to a redesign of the basic gun system. The addition of a mixing chamber (Figure 10) has greatly reduced the erosion problem. The choice of a low-molecular-weight propelling fluid has greatly reduced the temperature of the fluid to which the wall is exposed without degrading gun performance.

This temperature control has allowed the Electrothermal gun to operate in temperature regimes comparable with conventional guns. However the ET gun performance is significantly improved (Figure 5), when compared to conventional gun performance. This is because of its ability to used shaped power pulses and its use of low-molecular-weight propelling fluids which have higher sound speed and thus more efficient coupling from the breech to the projectile.

In the Electromagnetic (rail) gun, the plasma appears directly behind the projectile. Therefore no "mixing chamber" design is possible. The insulators ablate as a result of the heating, and rails may also, though to a lesser extent (Table 1).

40

This ablated material adds to the accelerated mass, reducing the efficiency of projectile acceleration.

Both Electrothermal and Electromagnetic guns appear capable of reaching higher velocities than conventional powder guns. Both have demonstrated this in the laboratory. However, the relevant measure is the weaponizability of the resulting device.

The conventional EM gun is subject to a wall erosion problem that appears unavoidable. As a result, military operation would require replacement of the barrel after a few, or perhaps up to 30 shots.

The recent redesign of the Electrothermal gun has greatly reduced barrel erosion. Present designs of upgraded ET guns use pressures and temperatures comparable with present 120 mm and 155 mm powder guns, and shorter acceleration times. Thus barrel lifetimes equal or longer than conventional guns are predicted.

List of references

1. A. E. Seigel, "Theory of High-Muzzle-Velocity Guns," in Interior Ballistics of Guns, Ed. H. Krier (New York: Am. Inst. of Aero. and Astro., 1979).

2. D. A. Tidman and S. A. Goldstein, "Thermal Transport to Hypervelocity Gun Tubes by High Pressure Partially Ionized Gas Flows," Technical Note GTD 85-4 (1985).

3. L. Spitzer, Jr., Physics of Fully Ionized Gases (New York: Interscience, 1962).

4. D. L. Book, NRL Plasma Formulary, NRL Pub. 0084-4040 (Washington, DC, Revised 1986), p. 38

5. S. I. Braginskii, Reviews of Plasma Physics, Ed. M. A. Leontovich (New York: Consultants' Bureau, 1965), p. 216

6. D. A. Tidman, N. K. Winsor and S. A. Goldstein, "Gun Interior Ballistics Model for Constant Acceleration Launch of Projectiles," GT-Devices Technical Note GTD 86-2 (1986).

7. P. M. Morse and H. Feshback, Methods of Theoretical Physics (New York: McGraw-Hill, 1953), p. 1590.

8. P. R. Garabedian, Partial Differential Equations (New York: John Wiley, 1964), p. 151.

9. The T-4 Group, Sesame '83: Report on the Los Alamos Equation-of-State Library, Los Alamos National Laboratory Report LALP-83-4 (1983).

APPENDIX A

GUN INTERIOR BALLISTICS MODEL FOR CONSTANT

ACCELERATION LAUNCH OF PROJECTILES

D. A. TIDMAN, N. K. WINSOR AND S. A. GOLDSTEIN

GT-Devices
5705A General Washington Drive
Alexandria, VA 22312

Technical Note GTD 86-2

February 1986

CONTENTS

1. INTRODUCTION

A simple model for the interior gas flow inside the barrel of a gun is constructed. The approach is to consider the case of a projectile accelerated at constant acceleration due to a constant base pressure, and then to determine the gas flow that must be supplied at the gun tube entrance to sustain this constant acceleration. The effects of skin friction between the gas flow and the bore, as well as thermal transport from the gas to the bore, are included. Of these, skin friction has the most important effect on gun efficiency due to its contribution to pressure drops along the gun tube. The model is particularly suited for electrothermal guns[1] where the power is injected electrically into the chamber and can be well controlled as a function of time.

2. ACCELERATING PRESSURE RAMP MODEL

We seek an approximate solution in which the projectile velocity V_p undergoes uniform acceleration, g, and the fluid velocity deviates only slightly from spatial uniformity between the projectile base and the gun tube entrance. The fluid velocity is written in the laboratory frame,

$$\begin{cases} V = V_p(t) + v(x,t) \\ V_p = gt \\ v\left(\frac{1}{2} gt^2, t\right) = 0. \end{cases} \tag{1}$$

It is convenient to view the pressure profile in the gun in a frame of reference in which the projectile is at rest at the origin (Figure 1)
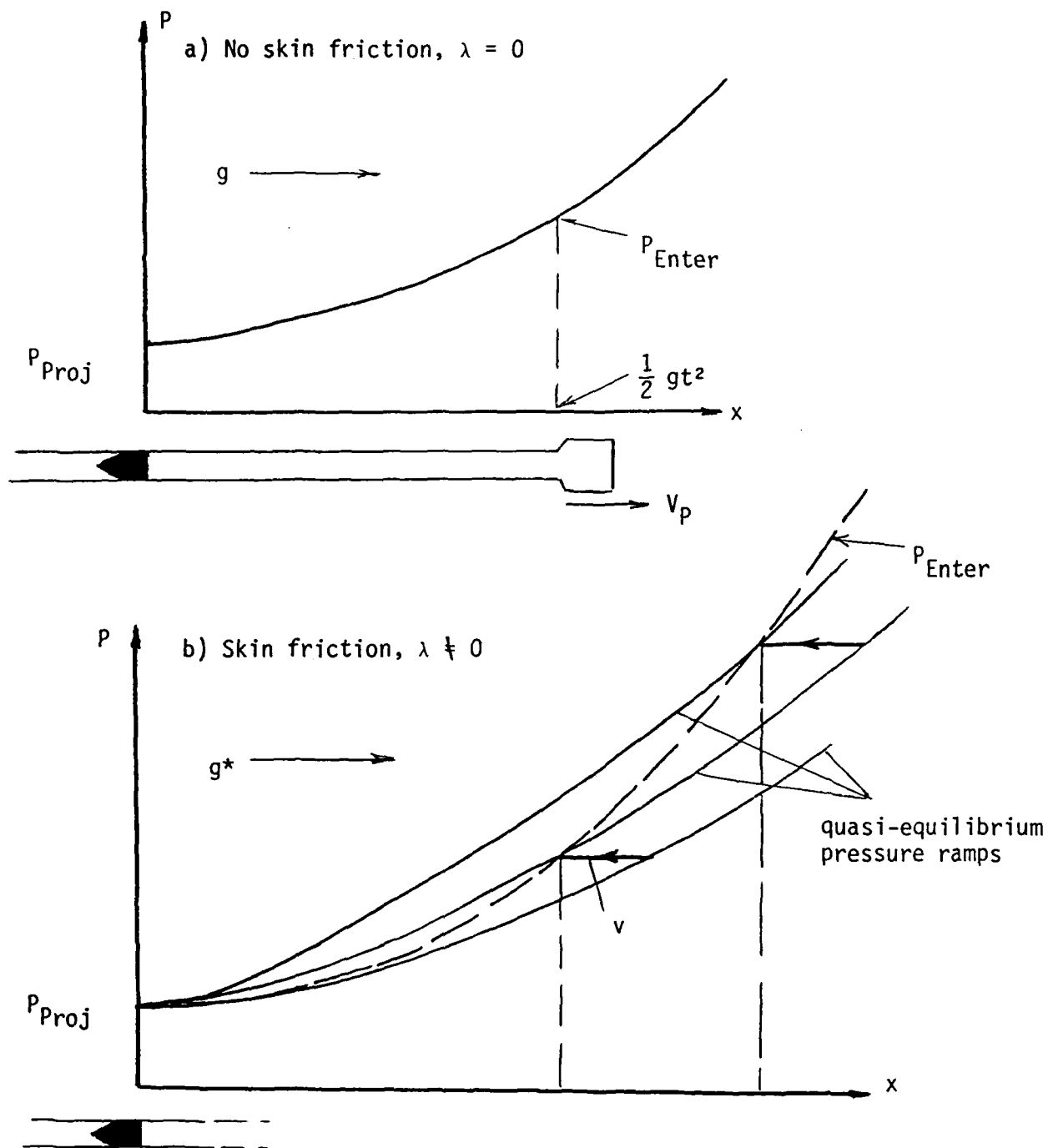
<u>Figure 1</u>

Pressure ramps behind a uniformly accelerating projectile (a) in the absence of skin friction and (b) with skin friction. Note, x is measured back from the projectile base in a frame at rest on the projectile and a uniform gravitational force per unit mass, g, acts on the gas.

2

with its constant base pressure P_{Proj}. In this frame the barrel slides past the projectile along the x axis at velocity gt and the gas experiences a gravitational field

$$g = \frac{A \, P_{Proj}}{M_{Proj}} \, , \qquad (2)$$

where $A = \pi a^2$ is the gun bore cross-sectional area.

2.1 Limit of Zero Coupling between Gun Tube Wall and Gas Flow

In this simple limit the only force on the gas is the uniform gravitational field (2) so that the pressure ramp in Figure 1a is $P = P_{proj} \exp(x/h_0)$, where the scale height $h_0 = c_s^2/\gamma g$ with c_s the sound speed. The velocity of the gas in the laboratory frame is $V(t) = gt$ with $v = 0$ for this example, and provided the gun tube entrance is fed with gas of pressure $P(x = gt^2/2)$ and velocity $V_p(t)$ the self-accelerating ramp of gas maintains the constant pressure P_{proj} on the projectile base.

2.2 Model Including Skin Friction and Wall Losses

Gas-wall interactions[2] give rise to important effects which will now be included approximately. The largest effect (assuming no ablation) is the skin friction force per unit mass acting on the gas, $\lambda V^2/2d$, where the friction coefficient λ is,

$$\lambda = \left\{ 2 \, \log_{10} \left(\frac{a}{\delta a_w} \right) + 1.74 \right\}^{-2} \qquad (3)$$

and δa_w is the roughness scale height of the gun bore of diameter $d = 2a$. This friction term gives rise to the velocity $v(x,t)$ in equation (1), and both λ and v are treated as small and of the same order, i.e., $\lambda \sim v \sim 0(\epsilon)$. To first order the skin friction per unit mass is thus

3

$\lambda V_p^2/2d$. It behaves like a slow time dependent increase in the acceleration factor g occurring in the scale height formula. Provided the "exponential atmosphere" can adjust its scale height h rapidly to these slow changes in g, the pressure ramp in the presence of skin friction can be viewed as evolving through a series of quasi-equilibrium states given by

$$\frac{1}{\rho}\frac{\partial P}{\partial x} = \frac{c_s^2}{\gamma}\frac{\partial}{\partial x}\ell n P = g + \frac{\lambda V_p^2}{2d} \,, \tag{4}$$

so that

$$\begin{cases} P(x,t) = P_{Proj}\exp\left(\frac{x}{h}\right) \,, \\[2mm] h(t) = \frac{c_s^2}{\gamma g^*} \,, \quad g^* = g\left(1 + \frac{\lambda V_p^2}{2gd}\right) \,. \end{cases} \tag{5}$$

The quasi-equilibrium model (4) applies provided the scale height h becomes shorter due to skin friction with a speed satisfying $dh/dt < c_s$ so that the pressure ramp (5) can adjust via local sound wave propagation. This condition becomes $t < \gamma d/\lambda c_s$ after which time V_p increases to the point where the ramp can no longer completely adjust.

In order to evolve the series of ramps (5) the gas must have a velocity v (in the frame of Figure 1b) given by

$$v(x,t) = \left(\frac{\partial x}{\partial t}\right)_p \approx -\left(\frac{\lambda V_p}{d}\right) x \,. \tag{6}$$

The entrance pressure P_{Enter} then evolves along the dotted path shown in Figure 1b.

4

Heat loss from the gas to the bore is also occurring but has a less important effect on the scale height h. It will be accounted for later in the energy balance.

3. ENERGY INPUT AND EFFICIENCY OF THE GUN

We now view the gun in the laboratory frame (Figure 2). Gas flowing into the gun tube entrance must carry sufficient energy to "fill out" the series of self-accelerating quasi-equilibrium ramps (5). We assume this input power continues for a pulse time τ after which it tapers off. The total energy that resides in the gun at a time $t < \tau$ can thus be written using (5) and (6) and integrating from $x = 0$ to $x_p = V_p^2/2g$ for the barrel contributions,

$$W_{input} = \frac{A\ P_{Proj} h}{(\gamma-1)} \left(e^{x_p/h} - 1 \right) + \frac{1}{2}\ A\rho_{Proj} h\ V_p^2 \left\{ \left(e^{x_p/h} - 1 \right) \left(1 - \frac{2\lambda h}{d} \right) \right.$$

(gas internal energy)

$$\left. + \frac{2\lambda x_p}{d} e^{x_p/h} \right\} \quad (7)$$

(gas kinetic energy)

$$+\ A\ P_{Proj} x_p \quad + \quad \frac{A\ x_{eff} P_{Enter}(t)}{(\gamma-1)} \quad + Q(t) \quad ,$$

(projectile KE)   (energy in chamber) (loss to wall)

where the effective chamber length x_{eff} is defined by

$$A\ x_{eff} = \pi a^2 x_{eff} = \text{chamber volume}, \quad (8)$$

and $\rho_{Proj} = \gamma P_{Proj}/c_s^2$. The entrance pressure into the gun tube is from (5),
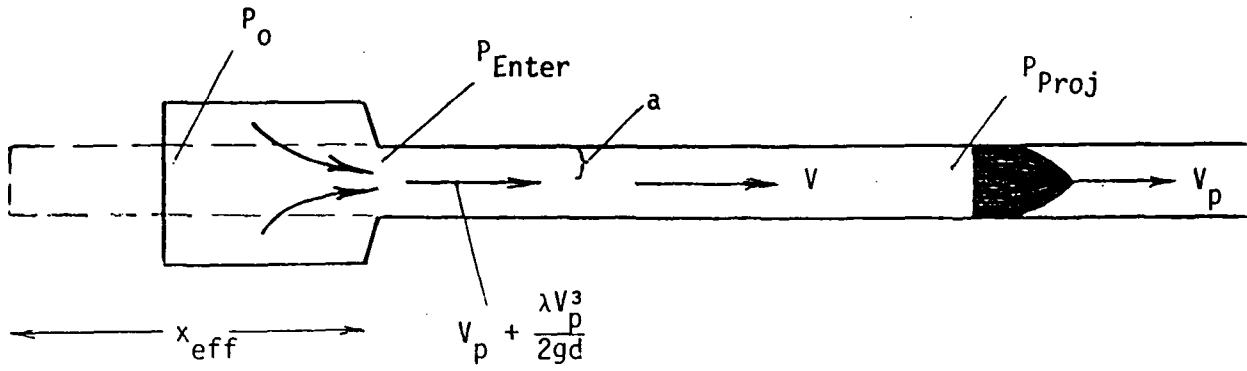
5

Figure 2

Parameters for an accelerating gas ramp in a gun tube.

$$P_{Enter} = P_{Proj} \exp\left\{ \frac{\gamma V_p^2}{2c_s^2} \left(1 + \frac{\lambda V_p^2}{2gd} \right) \right\} , \qquad (9)$$

and in the laboratory frame (Figure 2) the gas flow follows from (6) as,

$$V_{Enter} = V_p + \frac{\lambda V_p^3}{2gd} , \qquad (10)$$

and pressure drops between the chamber interior and gun tube entrance are neglected in the chamber energy. It is also interesting to note that if we use V_{Enter} and P_{Enter} to calculate a power flow into the gun tube and integrate it from 0 to t, a result slightly different from the barrel part of (7) is obtained. This is because the quasi-equilibrium ramps are not exact solutions to the flow equations.

To evaluate thermal loss to the tube wall we use the convective transport formula,[2]

$$q = \frac{10^{-3}\gamma}{(\gamma-1)} \phi PV \left(\frac{T - T_{Wall}}{T} \right) \; \text{ergs/cm}^2/\text{sec} , \qquad (11)$$

which gives

$$Q(t) = \int_0^t dt' \int_0^{x_p(t')} dx \; q \approx \frac{2\pi a}{(\gamma-1)} \gamma \phi \; 10^{-3} h^2 \; P_{Proj} \left\{ e^{x_p/h} - 1 - \frac{x_p}{h} \right\} , \qquad (12)$$

6

where we assumed $(T - T_{Wall})/T \approx 1$ (T = gas temperature). The function Φ appearing in (11) and (12) is discussed in Ref. 2, Eq. (3.19), and is about 1.5 for neutral gas and smooth bore gun tubes. Heat transfer to the chamber wall will be neglected.

3.1 Choked Flow Limit to V_{Enter}

The maximum velocity with which gas can flow into the barrel from a chamber of chambrage > 1 is the sound speed. The steepening pressure ramps can thus continue to be fed at the entrance provided from (10),

$$\left(\frac{\lambda c_s^2}{2gd}\right)\left(\frac{V_p}{c_s}\right)^3 + \left(\frac{V_p}{c_s}\right) - 1 \leqslant 0 \ ,$$

i.e., the pulse time τ must satisfy

$$\tau \leqslant \tau_{choke} = \frac{\dot{c}_s}{g}\left(\frac{V_p}{c_s}\right)_{choke} \ , \tag{13}$$

where

$$\left(\frac{V_p}{c_s}\right)_{choke} = y^{1/3}\left\{\left[\left(1 + \frac{8y}{27}\right)^{1/2} + 1\right]^{1/3} - \left[\left(1 + \frac{8y}{27}\right)^{1/2} - 1\right]^{1/3}\right\} \tag{14}$$

with

$$y = \frac{dg}{\lambda c_s^2} \ . \tag{15}$$

The quantity $(V_p/c_s)_{choke}$ is graphed as a function of y in Figure 3.
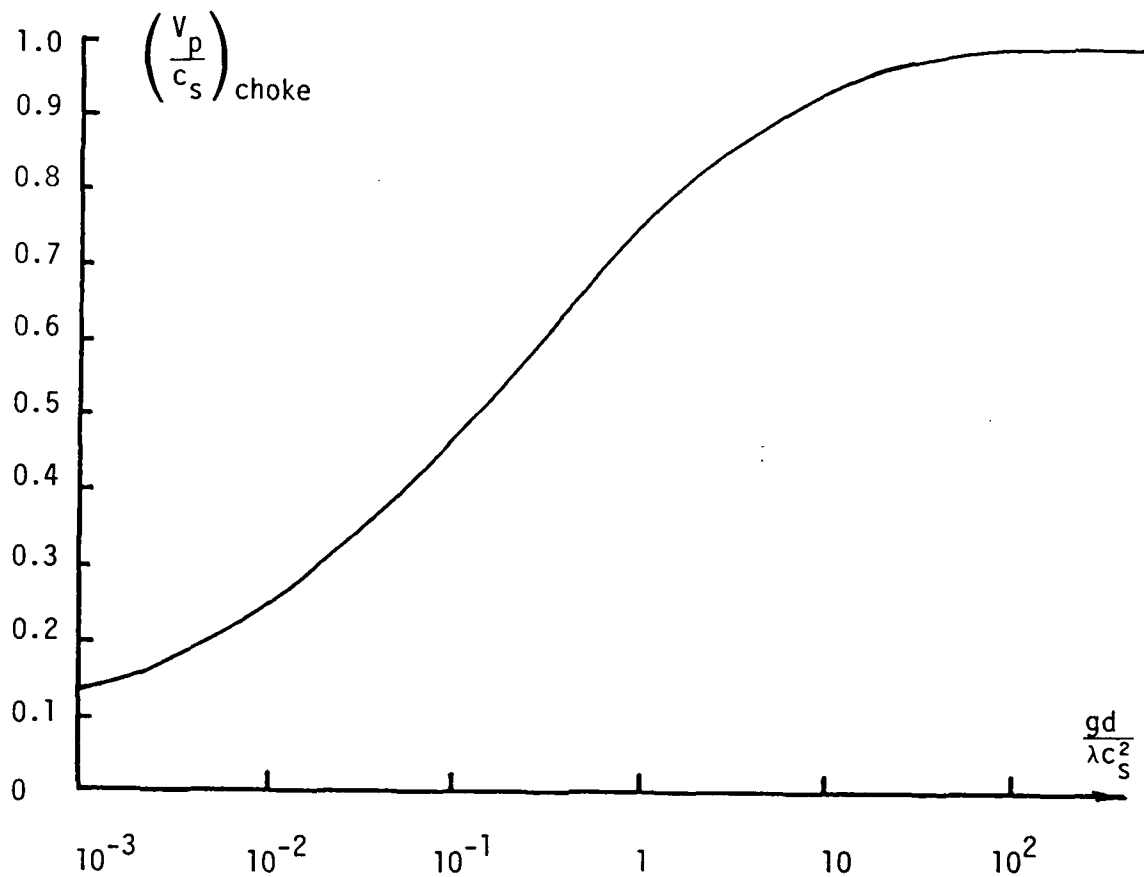
7

<u>Figure 3</u>

Projectile velocity V_p divided by the sound speed c_s at the time in its acceleration that gas flows into the gun tube entrance at the sound speed. Note that a small acceleration, g, and a large skin friction coefficient λ, causes the projectile velocity to reach only a small fraction of c_s when the choked flow limit c_s is encountered at the gun tube entrance.

8

3.2 Rarefaction Time, Projectile Energy, and Efficiency

Projectile acceleration continues beyond the power input time τ. Assuming the input power is reduced rapidly after τ, a rarefaction travels from the chamber down the gun tube to the projectile base where a deeper rarefaction is reflected. In order to launch a strong rarefaction into the barrel (so that no further appreciable acceleration occurs after its arrival at the projectile base) we first note that it takes a time $x_{eff}/2V_{Enter}$ for the chamber to drop its pressure by 0.5 after pulse shutdown. Since the projectile has advanced to a distance $g(\tau + x_{eff}/2V_{Enter})^2/2$ by this time, the total time τ_{Rare} for the rarefaction to reach the projectile is

$$\tau_{Rare} = \frac{g}{2c_s}\left(\tau + \frac{x_{eff}}{2V_{Enter}}\right)^2 + \frac{x_{eff}}{2V_{Enter}} \approx \frac{\tau}{2}\left(\frac{V_{p\tau}}{c_s}\right) + \frac{x_{eff}(V_{p\tau} + c_s)}{2c_s V_{Enter,\tau}} \quad , \qquad (16)$$

where the added subscript τ means quantities are evaluated at time τ.

The total energy acquired by the projectile is thus

$$W_{Proj} = \frac{1}{2} M_{Proj} V_F^2 \quad , \qquad (17)$$

where the projectile's final velocity is

$$V_F = g(\tau + \tau_{Rare}) \quad , \qquad (18)$$

which using (10) and defining

$$\beta = \frac{V_{p\tau}}{c_s} \qquad (19)$$

gives

$$\frac{V_F}{c_s} = \beta + \frac{\beta^2}{2} + \frac{gx_{eff}}{2c_s^2} \left\{ \frac{1 + \beta}{\beta + \left(\frac{\lambda c_s^2}{2gd}\right)\beta^3} \right\} , \tag{20}$$

and we note β has a maximum given by (14) for pulses of maximum length τ_{choke}.

The gun efficiency can now be written as

$$\epsilon = \frac{W_{Proj}}{W_{input}(\tau) + W_{late}} , \tag{21}$$

where W_{input} is given by (7) and W_{late} is the energy input to the gun occurring after the peak power input time τ.

4. SUMMARY OF FORMULAS

It is useful to define some dimensionless quantities

$$\theta = \frac{x_{eff}}{c_s \tau} , \qquad \psi = \frac{\lambda \tau c_s}{2d} , \qquad \beta = \frac{V_{p\tau}}{c_s} = \frac{g\tau}{c_s} . \tag{22}$$

The efficiency (21) then becomes,

$$\epsilon = \frac{0.5(\gamma-1)}{\Lambda} \left(\frac{V_F}{c_s}\right)^2 \frac{\gamma(1 + \psi\beta)}{\left(1 + \frac{W_{late}}{W_{input}}\right)} , \tag{23}$$

$$\Lambda = \left\{ 1 + \frac{1}{2} \gamma\beta^2(\gamma-1)[1 - \frac{4\psi}{\gamma\beta} + 2\beta\psi] + \theta\beta\gamma(1+\psi\beta) + \frac{2.10^{-3}\phi}{\beta(1+\psi\beta)} \left(\frac{\tau c_s}{a}\right) \right\} \times$$

$$\exp\left[\frac{\gamma\beta^2}{2}(1+\psi\beta)\right] + \left\{ \frac{1}{2}\gamma(\gamma-1)\beta^2(1+\psi\beta) - 1 - \frac{1}{2}\gamma\beta^2(\gamma-1)(1 - \frac{4\psi}{\gamma\beta}) \right. \tag{24}$$

$$\left. - \frac{2.10^{-3}\phi}{\beta} \frac{\tau c_s}{a} \left[\frac{1}{(1 + \psi\beta)} + \frac{1}{2}\gamma\beta^2\right] \right\}$$

10

and the projectile final velocity V_F is given by

$$\left(\frac{V_F}{c_s}\right) = \beta + \frac{\beta^2}{2} + \frac{\theta}{2} \left(\frac{1+\beta}{1+\beta\psi}\right) \qquad (25)$$

and the formulas only apply for pulses of length

$$\frac{2x_{eff}}{\beta c_s} < \tau \leqslant \tau_{choke} = \frac{c_s}{g} \left(\frac{V_P}{c_s}\right)_{choke} \qquad (26)$$

given by (14), (15), and Figure 3. The lower limit on τ in (26) exists because the barrel hydrodynamics have been treated more accurately than the chamber hydrodynamics in this model. The condition is that the barrel volume $V_\tau \tau A/2$ should exceed the chamber volume $x_{eff} A$ for the model to apply, e.g., by a factor of 3 or more.

Other quantities of interest are the pressure ratio

$$\frac{P_{Enter}(t)}{P_{Proj}} = exp\left\{\frac{\gamma\beta^2}{2}\left(\frac{t}{\tau}\right)^2\left[1 + \psi\beta\left(\frac{t}{\tau}\right)\right]\right\} \qquad (27)$$

and the total mass of working fluid in the gun

$$M_{Fluid} = A\int_0^{x_{p\tau}} \frac{\gamma P(x)}{c_s^2} \, dx + Ax_{eff}\left(\frac{\gamma P_{Enter,\tau}}{c_s^2}\right)$$

$$= M_{Proj}\left\{\left[\gamma\theta\beta + \frac{1}{(1+\psi\beta)}\right]exp\left(\frac{\gamma\beta^2}{2}(1+\psi\beta)\right) - \frac{1}{(1+\psi\beta)}\right\}. \qquad (28)$$

M_{Fluid} fixes the minimum chamber size needed to contain this mass of

11

fluid at its original liquid or solid density.

Finally, consider the power input to the gun. At the end of the pulse time τ we assumed the fluid in both the barrel and the chamber to have the same γ. However, at early times the fluid in the chamber may have a different value, say γ_0, due to EOS effects such as molecular covolume. If we assume that the very early part of the power input pulse raises the chamber volume to pressure P_{Proj} before the projectile advances appreciably (say not more than about one bore diameter), then the above formulas are not sensitive to the fill-up pulse shape. The energy required in this early pulse is $Ax_{eff}P_{Proj}/(\gamma_0-1)$ and should be delivered in a time (Figure 4).

$$ t \gtrsim \tau_{Fill} = \left(\frac{2d}{g}\right)^{1/2} \tag{29} $$

After this the power input required is given by $\dot{W}_{input}$ from (7) until the end of the effective pulse time τ. Energy flowing in, W_{late}, for $t > \tau$ has little effect on the projectile due to the rarefaction catch-up and reflection. This late energy simply reduces the efficiency (23) or (21).

4.1 Gun Tube Entrance Heating

The gun tube entrance has a wall temperature T_w and receives heat from the gas flow of temperature T. Using Eq. (4.1) in Reference 2, this increases to $T_w(\tau)$ °K given by

$$ T_w(\tau) = T_w(0) + \frac{\alpha}{2} \int_0^\tau \frac{dt}{(\tau-t)^{1/2}} \frac{10^4 \gamma}{(\gamma-1)} \phi \left(P_{kb}V_{km/s}\right)_{Enter} \left(\frac{T - T_w(t)}{T}\right) $$
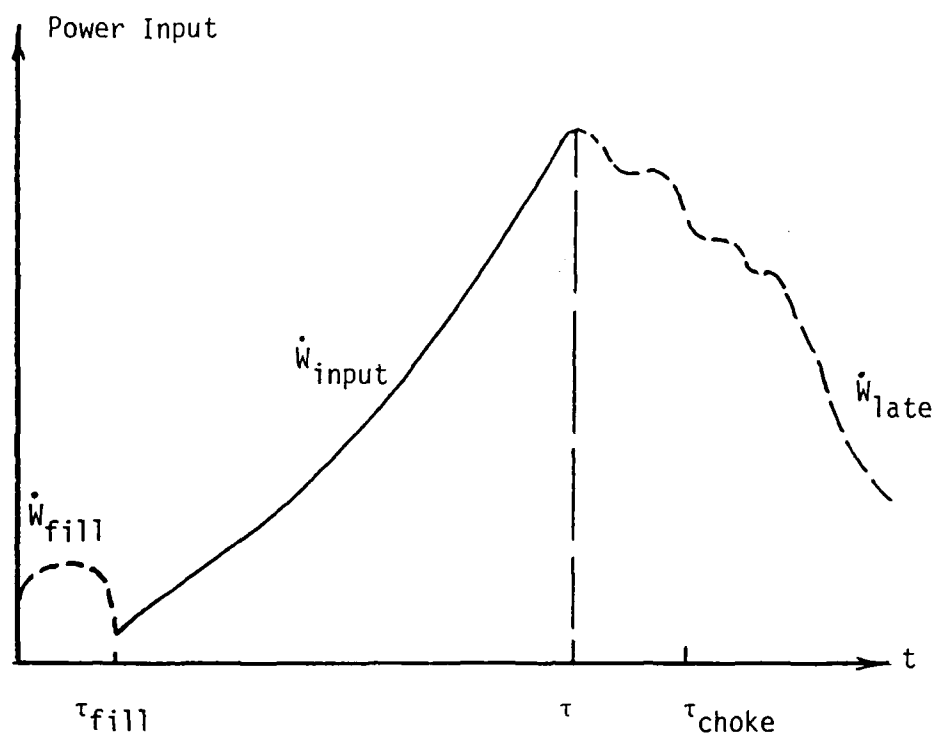
12

Figure 4

Input power to a gun showing the three components, namely (i) pressure
fill-up of the chamber, (ii) the constant acceleration gas ramp, and
(iii) the late wasted energy input the beginning of which launches a
rarefaction into the barrel. Note W_{late} includes all the energy input
for times t > smaller of τ or τ_{choke} and the case $\tau < \tau_{choke}$ is shown.

13

in the pulse time τ. We evaluate this in the same approximate manner as Reference 2 and find*using (9) and (10),

$$T_w = \frac{T_{wo} + T(\tau/\tau_{heat})^{1/2}}{1 + (\tau/\tau_{heat})^{1/2}} \qquad (30)$$

where

$$\tau_{heat} = \left\{ \frac{0.525 \, (\gamma-1)}{\alpha\gamma\Phi\beta \ c_s(km/s)} \quad \frac{(T(^\circ K)/3,500)}{P_{Proj}(kbar)exp\left[\frac{\gamma\beta^2}{2} \ (1+\psi\beta)\right]} \right\}^2 \text{seconds.} \quad (31)$$

This heating is severe and leads to the desirability of wall coatings at large bore sizes. High sound speeds, low pressures, low gas temperatures, high γ and small α are also desirable ($\alpha = 2/(\pi\rho_w c_w K_w)^{1/2}$ in units of cm² $^\circ$K sec$^{1/2}$/Joules). But low pressures cause low accelerations and the limits imposed by skin friction and choked flow (eq. 14) lower the gun performance and must be involved in the trade-offs.

5. NUMERICAL DISCUSSION

The sound speed c_s and specific heat ratio γ are important quantities for the propelling gas. The sound speed strongly determines the scale height h of the gas ramp (Eq. 5) which in turn limits the practical acceleration length for a given accelerating pressure P_{Proj}, the limit being set by the ability of the chamber to contain the entrance pressure and by the increased bore entrance heating (Eq. 30) that occurs if P_{Enter} becomes very large. The skin friction dependence of h (Eq. 5) also sets velocity limits for low mass projectiles accelerated over long lengths by low propelling pressures.

_____

*In Equations 4.5 and 4.6 of Ref. 1 set $t=\tau$ and $\tau=\tau_{heat}$ to align these results, but note the result (31) accounts for the barrel pressure ramp.

Figure 5 shows a plot of efficiency as a function of γ for a specific example. The model we have constructed assumes that both γ and c_s are given constants. However, they must be chosen to be consistent with the appropriate equation of state (EOS) for the working fluid and for the pressures and temperatures involved in the gun. Since the highest fluid pressure and energy density occur at the gun tube entrance at the end of the pulse, and this also controls the chamber energy and choking limit, the values of γ, c_s, evaluated at $P_{Enter}(\tau)$ provide a reasonable approximation for this choice. An iteration procedure could be used between the model equations (23) - (26) and EOS to select γ, c_s consistently with P_{Enter} and T. In the rest of this discussion we give an example, but use a simpler first step approximation to such an iteration process.

Figures 6 and 7 show the sound speed c_s and $(\gamma-1)$ for water (superheated steam) graphed as functions of temperature for several pressures[3]. The variation of $(\gamma-1)$ with P is relatively more important as can be seen by noting that for a fixed temperature, e.g., T = 3,273°K (0.28 eV)

$$(\gamma-1) \approx 0.169 + 0.021\, P_{kb} \quad , \qquad (32)$$

$$c_s(km/sec) \approx 1.356 + 0.074\, P_{kb} \quad .$$

To include this approximately in the expressions for ϵ, W_{input}, etc., we will replace γ by γ_{Enter} in the sensitive parts of the expressions (on the left side of the equations below) and set $\gamma = \bar{\gamma}$, $c_s = \bar{c}_s$ on the right where $\bar{\gamma}$, $\bar{c}_s$ are estimated means values for the insensitive parts of ϵ, W_{input}, etc. Thus,
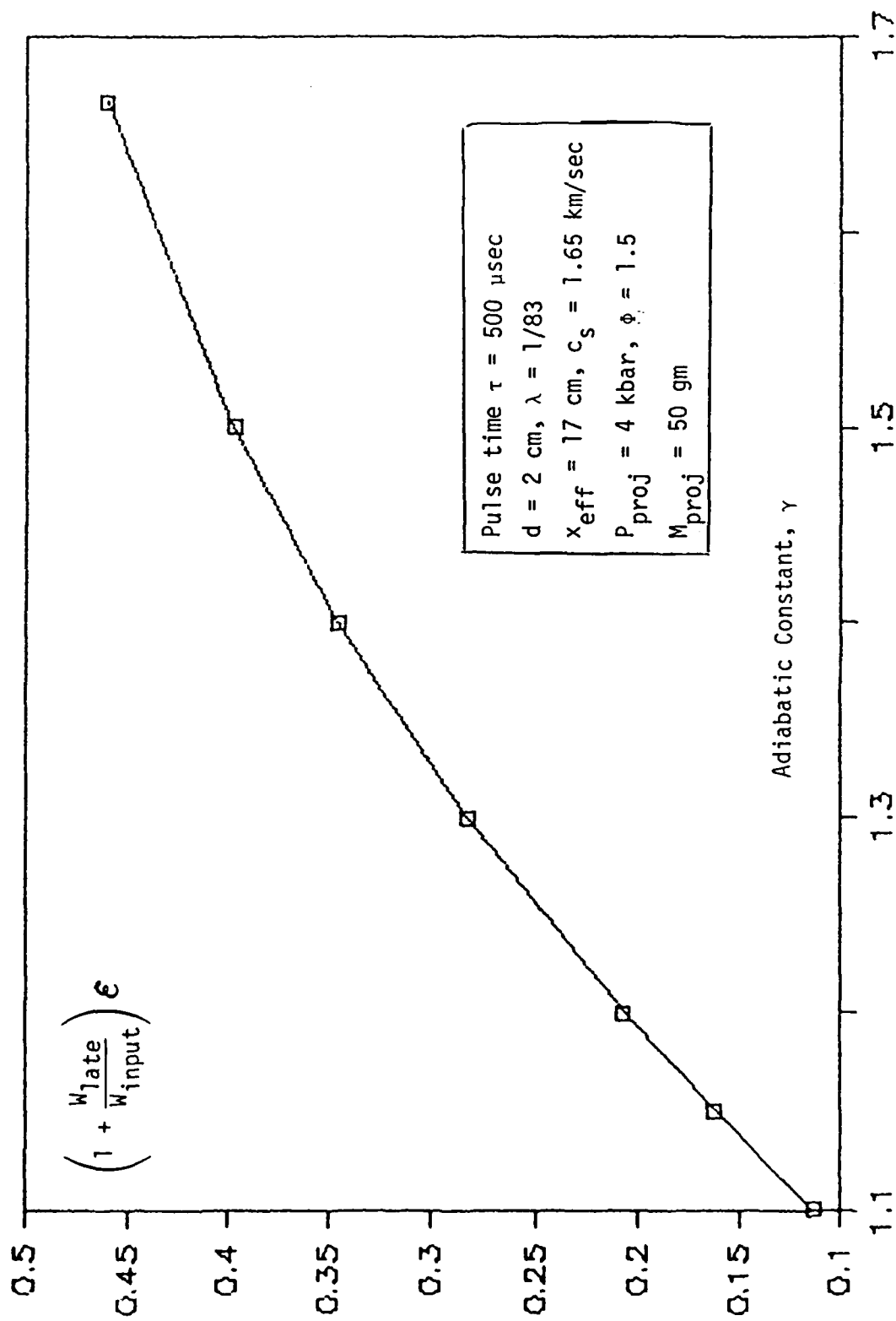
15

Figure 5

Graph giving the gun efficiency, ϵ, as a function of γ for a gun with the parameters indicated.

Chart details (axis labels and legend within the figure):

Y-axis: $\left(1 + \dfrac{W_{late}}{W_{input}}\right)\epsilon$

X-axis: Adiabatic Constant, γ

Legend:
Pulse time τ = 500 μsec
d = 2 cm, λ = 1/83
x_{eff} = 17 cm, c_s = 1.65 km/sec
P_{proj} = 4 kbar, ϕ = 1.5
M_{proj} = 50 gm

$$\frac{\epsilon}{(\gamma_{Enter}-1)} \approx \frac{0.5\ \bar{\gamma}(1+\psi\beta)}{\Lambda\left(1 + \frac{W_{late}}{W_{input}}\right)}\left(\frac{V_F}{c_s}\right)^2 \tag{33}$$

$$\frac{W_{input}(\gamma_{Enter}-1)}{M_{Proj}} \approx \frac{1}{2}\ \bar{c}_s^2\ \left(\frac{V_F}{c_s}\right)^2\ \left(\frac{\gamma_{Enter}-1}{\epsilon}\right) \tag{34}$$

$$P_{Enter} \approx P_{Proj}\ \exp\left\{\frac{\bar{\gamma}}{2}\ \beta^2\ (1 + \psi\beta)\right\} \tag{35}$$

$$g = \frac{P_{Proj}}{M_{Proj}}\ A \tag{36}$$

All quantities on the right are functions of,

$$\left\{a,\ \tau,\ x_{eff},\ \Phi,\ \lambda,\ \bar{\gamma},\ \bar{c}_s,\ \frac{P_{Proj}}{M_{Proj}}\right\} \tag{37}$$

in which $\bar{\gamma}$, $\bar{c}_s$, are estimated values and on the left of (33) and (34),

$$\gamma_{Enter} = \gamma(P_{Enter})\ , \tag{38}$$

where the example (32) for 3,273°K steam will be used. It should also be noted that for pulse times

$$\tau > \tau_{choke} = y^{1/3}\ \left\{\left[\left(1 + \frac{8y}{27}\right)^{1/2} + 1\right]^{1/3} - \left[\left(1 + \frac{8y}{27}\right)^{1/2} - 1\right]^{1/3}\right\}\ .$$

$$y = dg/\lambda\bar{c}_s^2 \tag{39}$$

the energy in that part of the pulse $W(\tau > \tau_{choke})$ is not effectively used for projectile acceleration and should be included in W_{late}. For these cases we simply set

$$\beta = \beta_{choke} = \frac{g\tau_{choke}}{\bar{c}_s} \tag{40}$$

throughout the formulas.

Using the above procedure, we have graphed several quantities of interest. Figure 8 shows the projectile velocity as a function of projectile mass for a 500 μsec input pulse time for the 20 mm gun parameters shown. All of the figures 9 to 15 give results for the optimum pulse length $\tau = \tau_{choke}$ for a gun with parameters listed in Figure 9. These examples are all for superheated steam at 3,273°K.

5.1 Model Limitations and Chamber Hydrodynamics

The model gives attention to the pressure ramp in the barrel and the entrance flow, with only rough accounting for the chamber hydrodynamics. Thus the model has useful accuracy for guns with small enough chambers so that the last term in Eq. 20 is small. However, a more exact treatment of the chamber hydrodynamics would require one to address a specific chamber since gun chambers are varied in geometry and internal structure. This is particularly the case for electrothermal guns that are designed to inject these constant acceleration ramps into the gun tube. Note also that an ideal power input pulse would be sharply cut off at τ as in Figure 15. However, realistic input power pulses would not cut off so sharply and continuing power input would slightly delay the rarefaction.

18

The 50% chamber pressure drop time used in Eq. 16 is an estimate for all these effects.

A second area where the model could be improved would be to allow the parameters γ and c_s in the scale height formula (5) to vary slowly with x. This would allow one to account for the pressure dependence of these quantities along the pressure ramp via the equation of state, and to also allow for a variation in the gas temperature $T(t)$ injected by more general pulse structures.
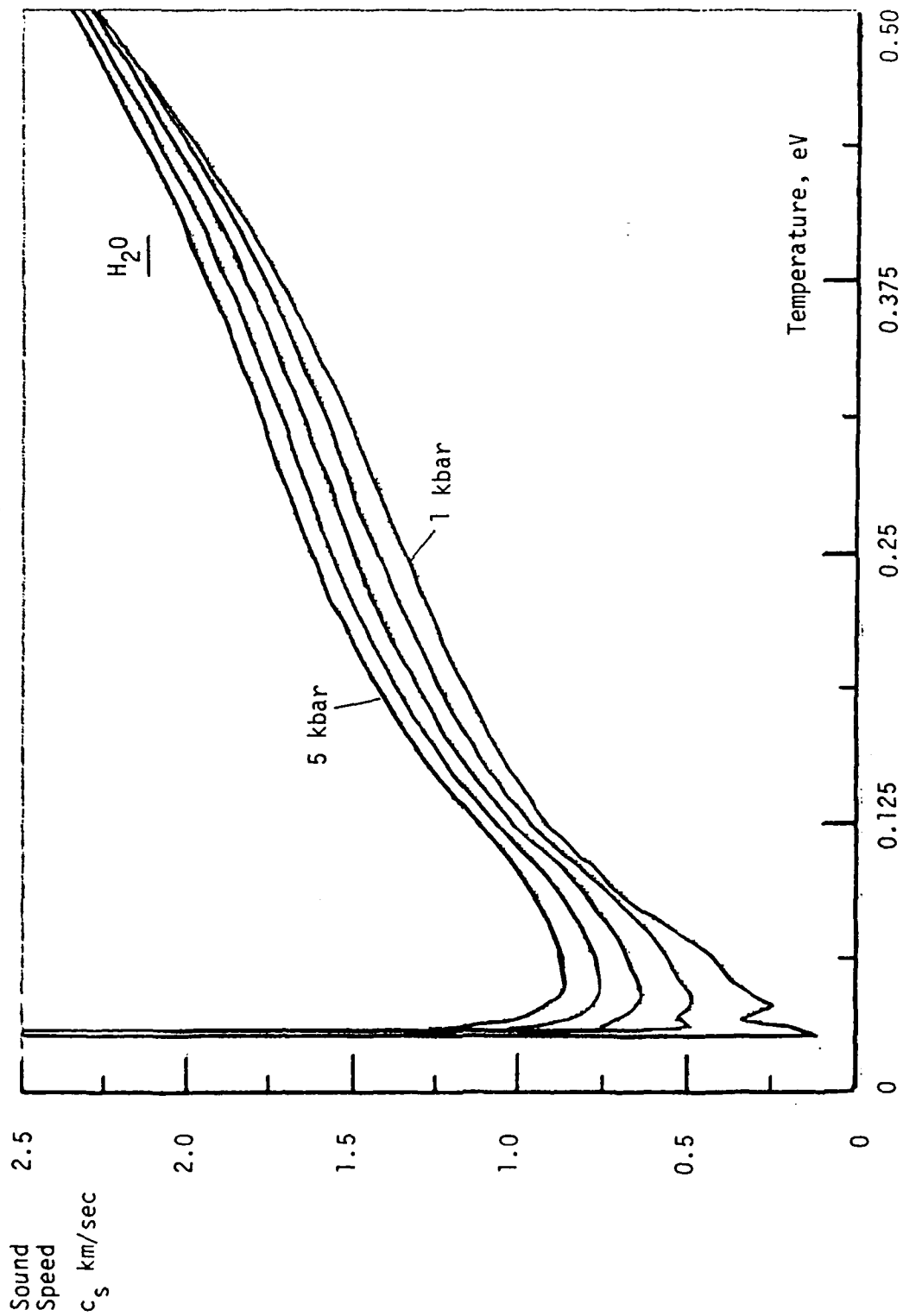
Figure 6

Sound Speed for Water

20
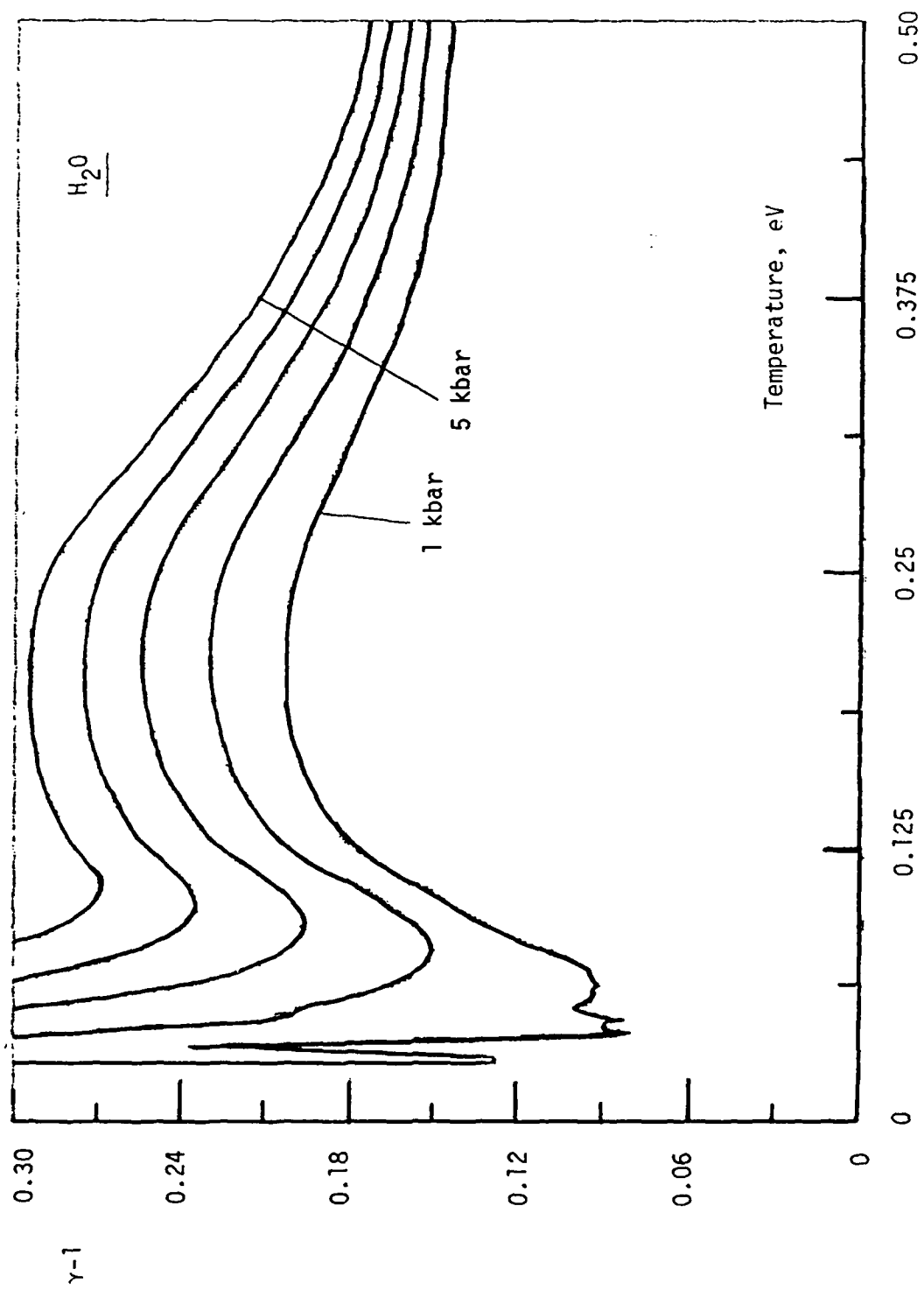
Figure 7

Equation of State data for water

21
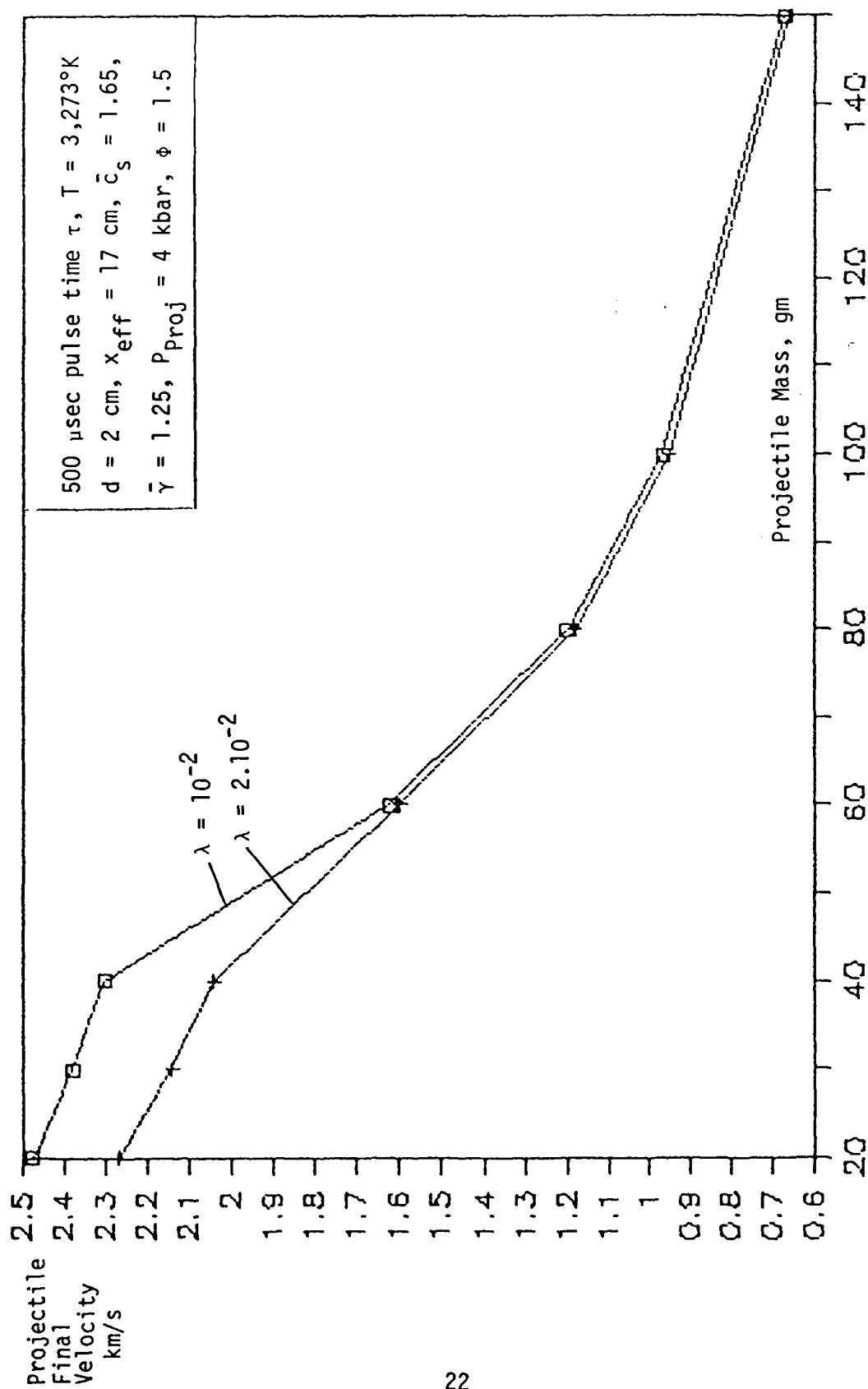
Figure 8

Graphs for a 20 mm gun with a 500 μsec input pulse time for two values of the skin friction coefficient λ. The working fluid is steam.
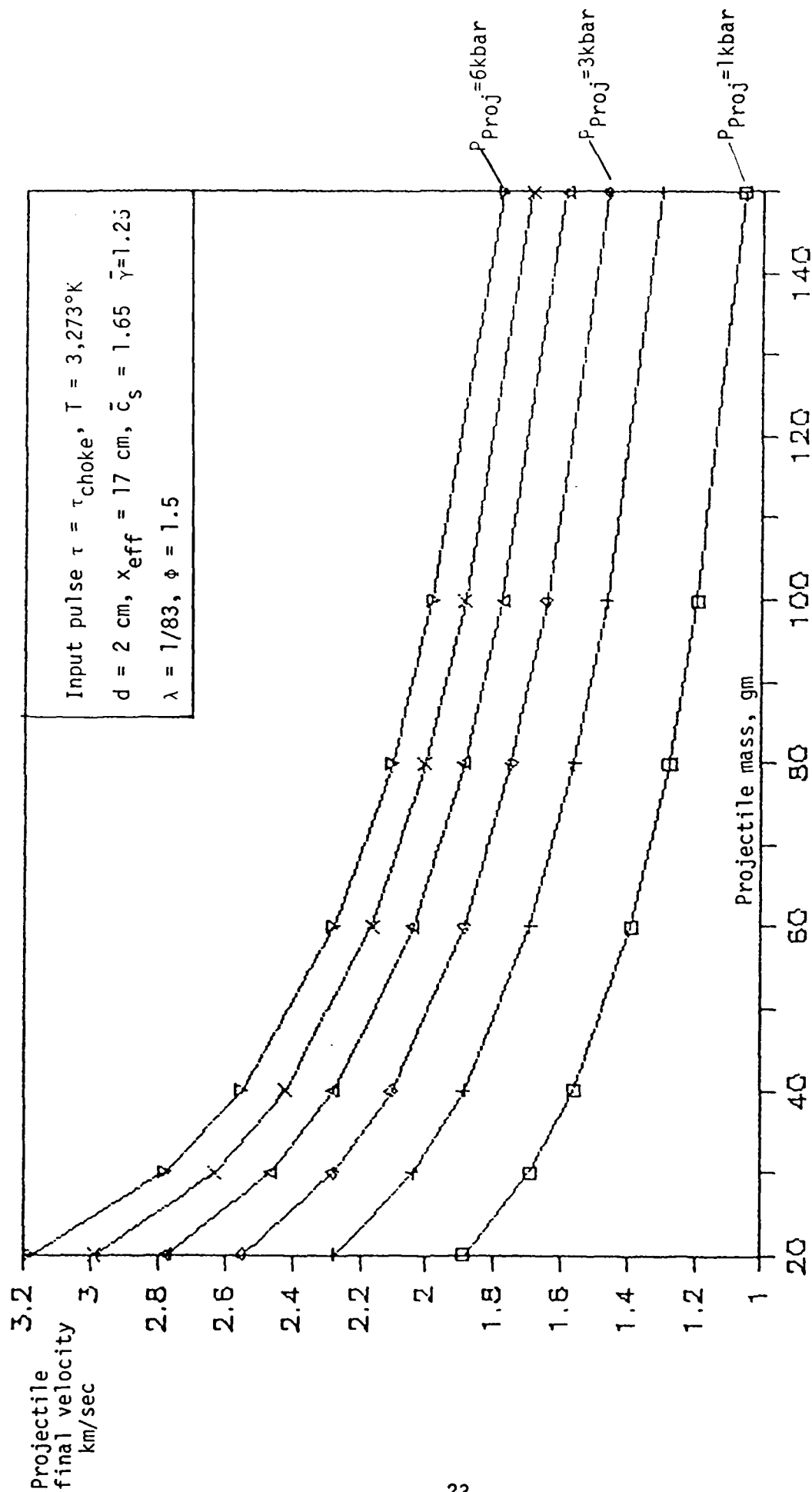
Figure 9

Projectile velocity as a function of projectile mass for several base pressures for input power pulses of length $\tau = \tau_{choke}$. The remaining figures 10 - 15 give other quantities for this same example.
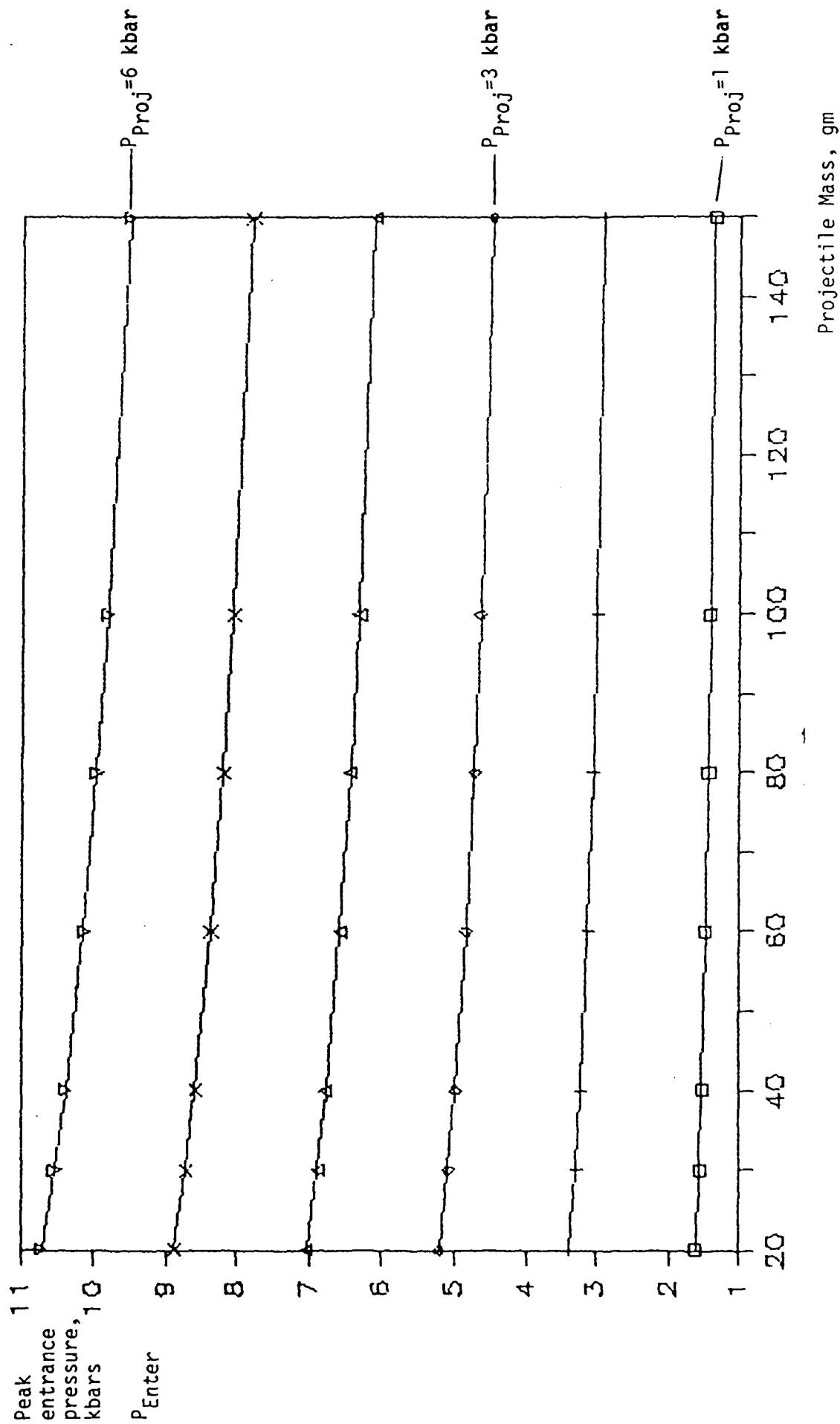
23

Figure 10

Peak entrance pressure as a function of projectile mass for several projectile base pressures for pulses of length $\tau = \tau_{choke}$ with gun parameters the same as in Figure 9.

24
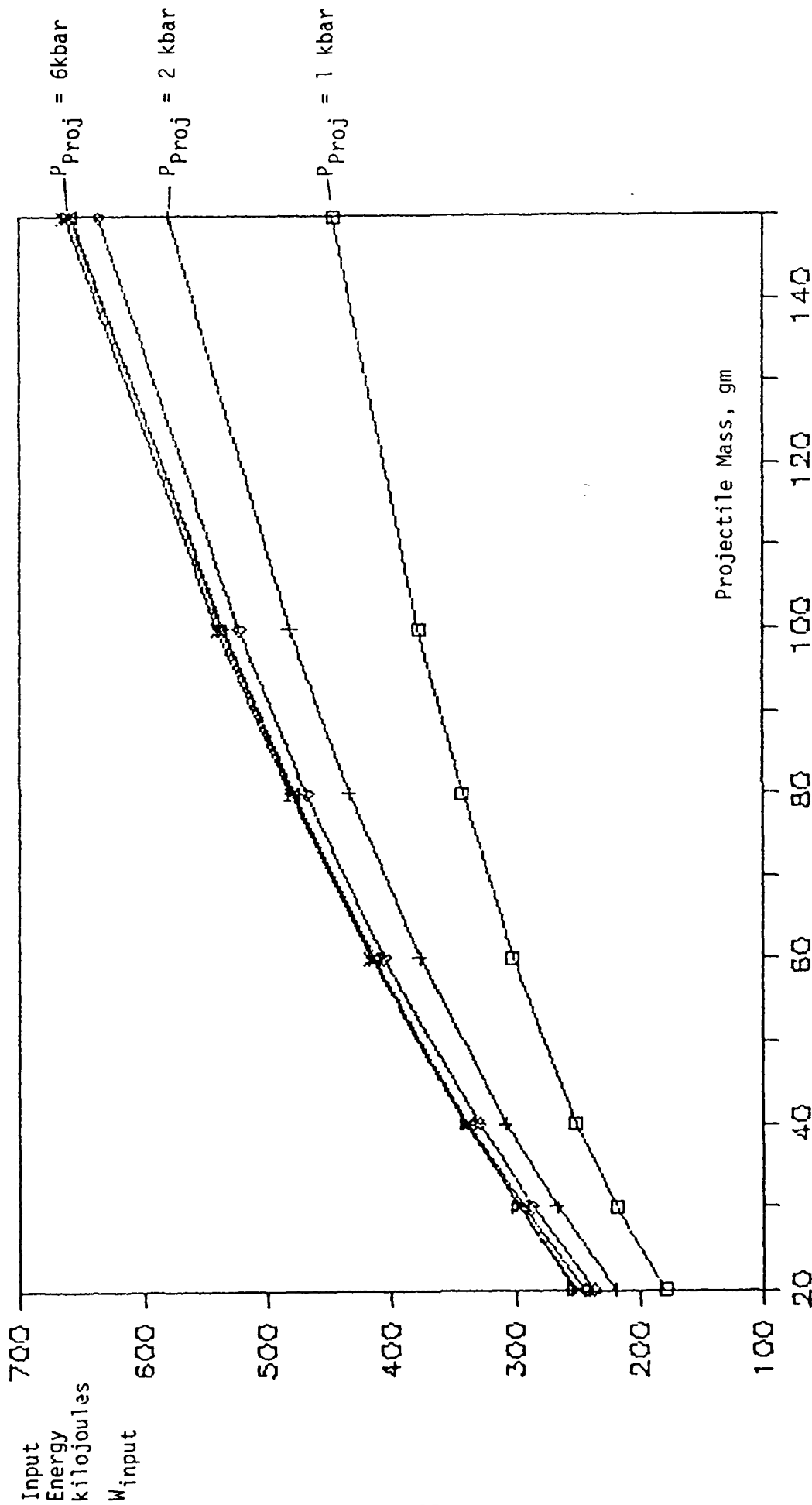
Figure 11

Input Energy, W_{input}, as a function of projectile mass for several projectile base pressures and pulses of length $\tau = \tau_{choke}$ with gun parameters the same as listed in Fig. 9.
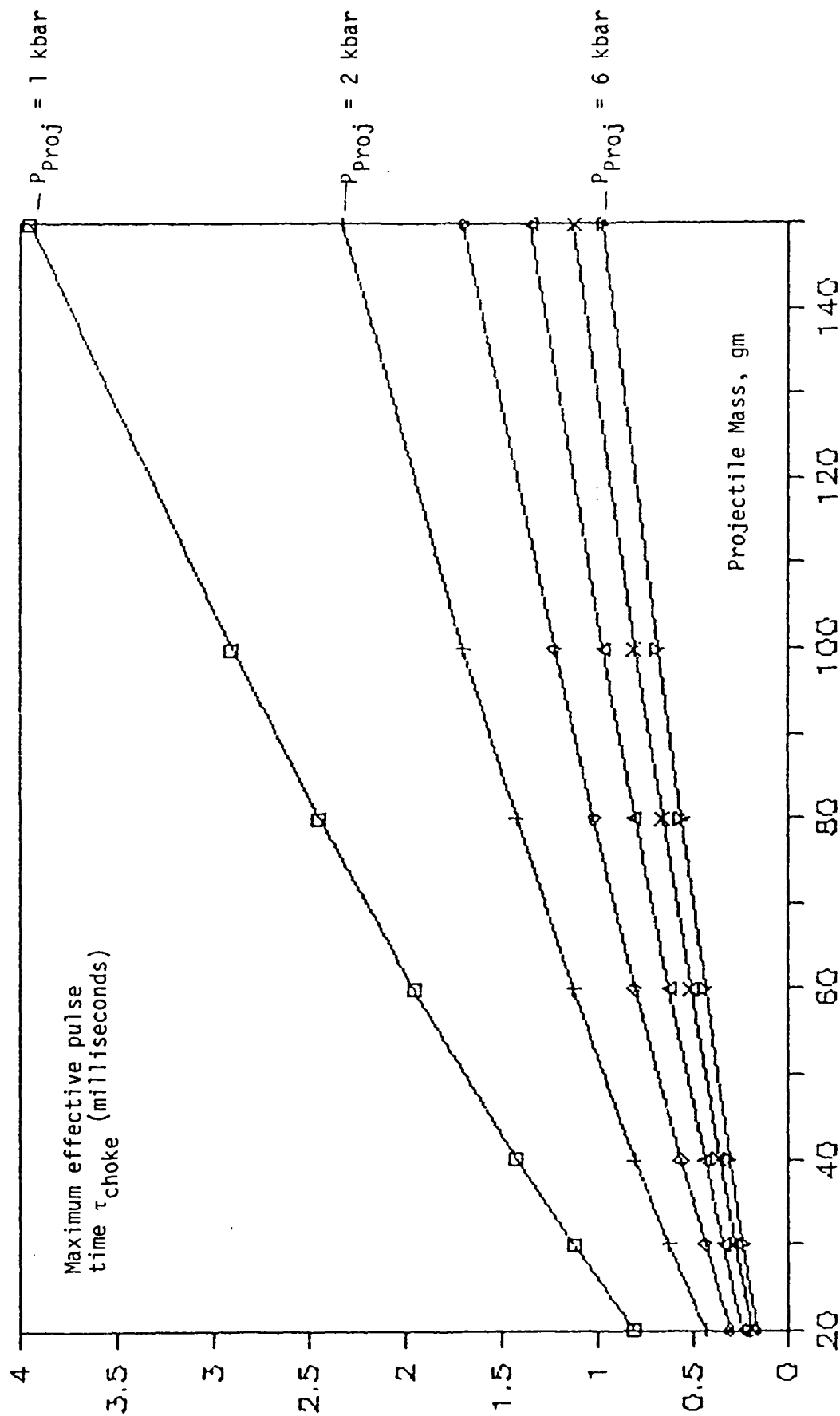
25

Figure 12

Maximum effective pulse time τ_{choke} as a function of projectile mass for several projectile base pressures with gun parameters the same as listed in Figure 9.
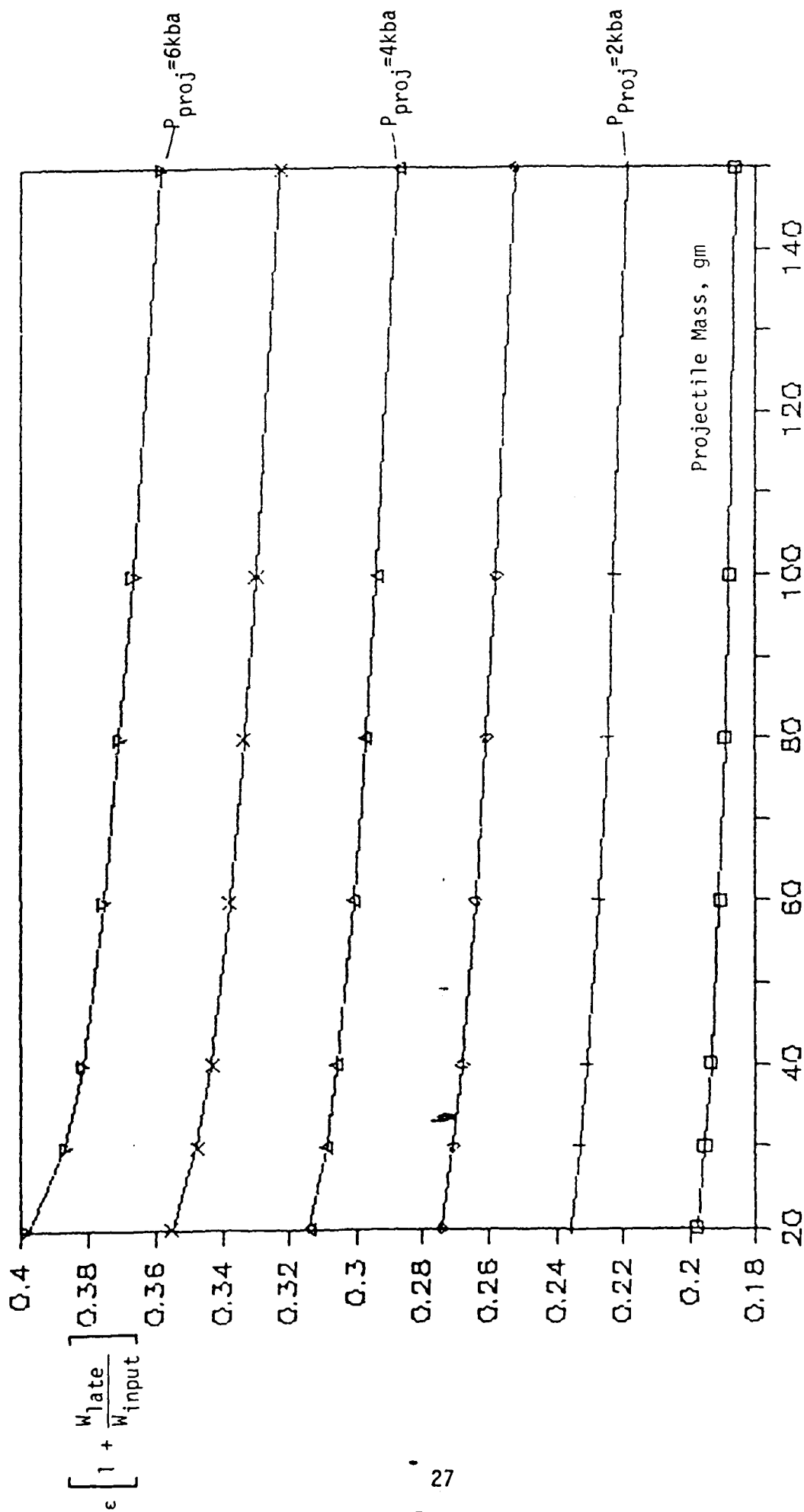
26

Figure 13

Graph giving the efficiency, ϵ, as a function of projectile mass for pulses of length $\tau = \tau(\text{choke})$ with gun parameters as in Figure 9. Note, for these "mass-matched" pulses the heavier masses involve smaller g's and larger pulse lengths $\tau(\text{choke})$. This gives larger acceleration lengths before encountering the choked flow limit at the tube entrance, which results in more skin friction and slightly lower efficiencies. For mismatched pulses of duration $\tau > \tau(\text{choke})$, eg., for small projectile mass, $W(\text{late})$ includes energy input for $\tau > \tau(\text{choke})$ which gives a small efficiency ϵ.
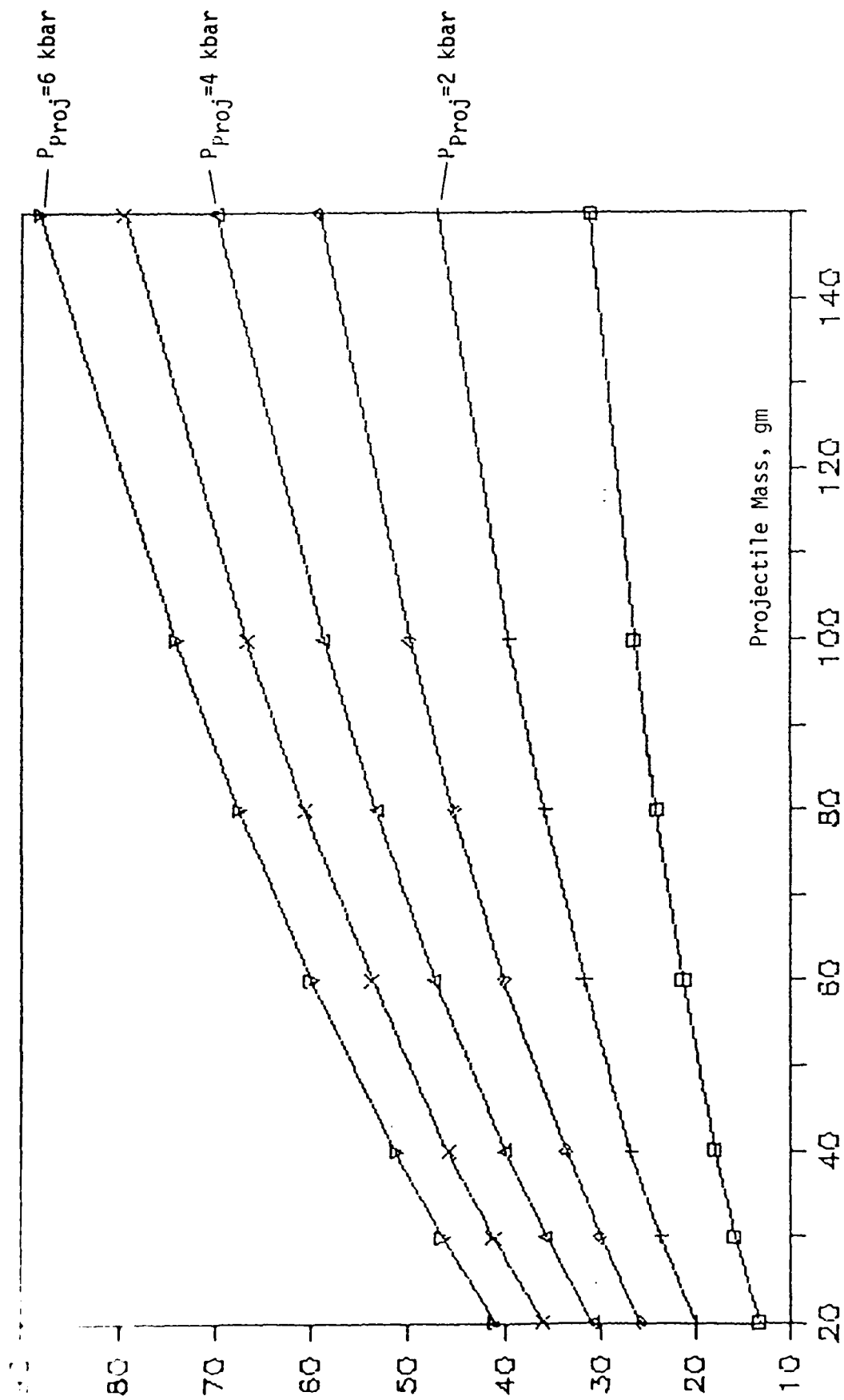
27

Figure 14

Mass of propellant fluid as a function of projectile mass for several projectile base pressures and pulses of length $\tau = \tau_{choke}$ with gun parameters the same as listed in Figure 9.
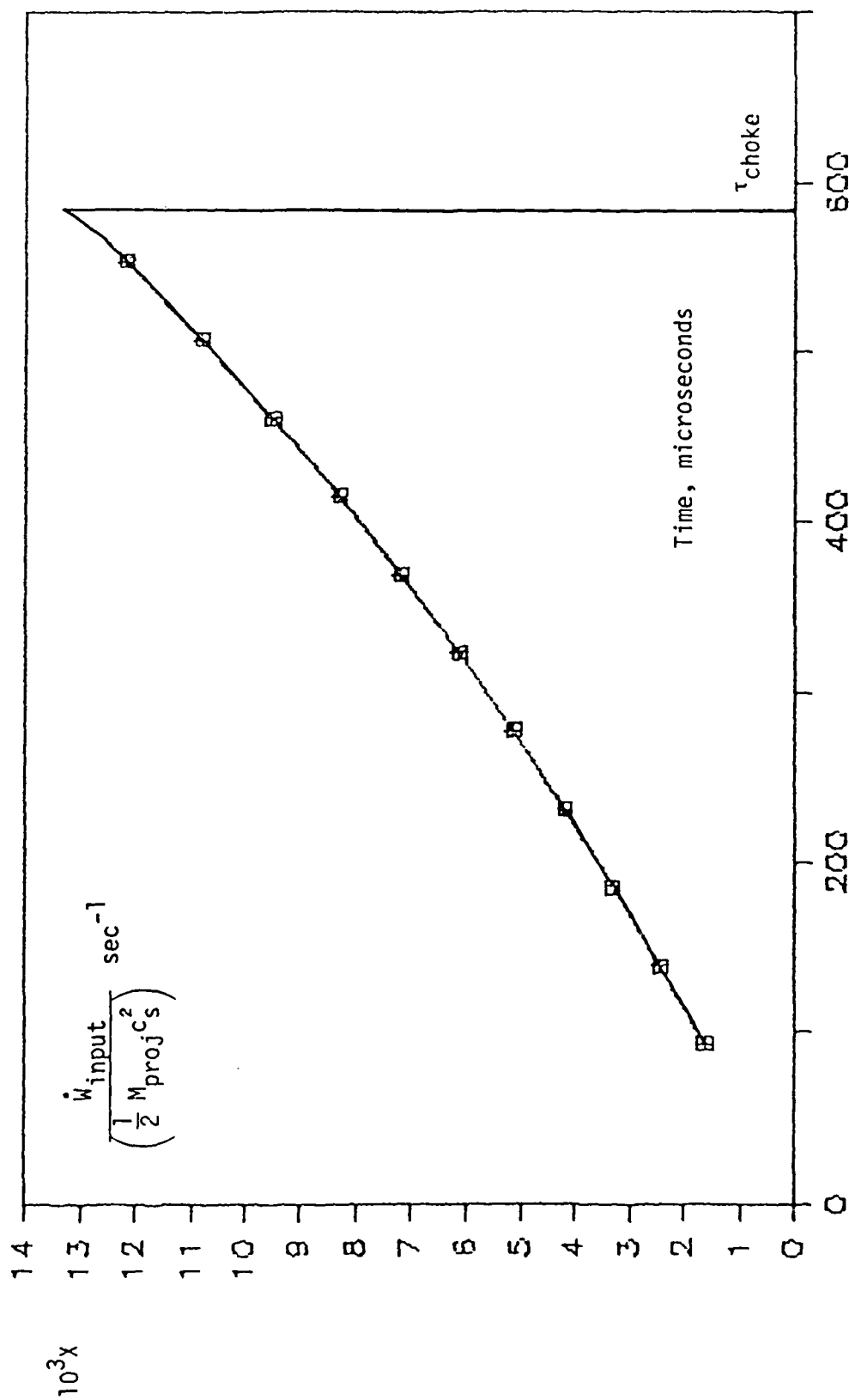
Figure 15

Power input in units of $M_{proj}c_s^2/2$ for 60 gram projectile with a base pressure of 4 kilobars accelerated in a gun with parameters the same as listed in Figure 9.

REFERENCES

1. S. A. Goldstein, D. A. Tidman, R. L. Burton, D. W. Massey, and N. K. Winsor, Electric Cartridge Guns Using Fluids Heated by a Capillary Plasma Jet, GT-Devices Report No. 83-11 (1983).

2. D. A. Tidman and S. A. Goldstein, Thermal Transport to Hypervelocity Gun Tubes by High Pressure Partially Ionized Gas Flows, GT-Devices Report No. 85-4 (1985).

3. Equation-of-State Data Listing, SESAME Tables, Los Alamos Science Liaison Company, 253 Rio Bravo, Los Alamos, NM 87544 (an information transfer service of LASL data).

END
FILMED

DATE: 7-92

DTIC